

Systematic Magnetic Structure Generation Based on Oriented Spin Space Groups: Formulation, Applications, and High-Throughput First-Principles Calculations

Takuya Nomoto ,^{1,*} Kohei Shinohara ,^{2,†} Hikaru Watanabe ,³ and Ryotaro Arita ,^{2,4}

¹*Department of Physics, Tokyo Metropolitan University, Hachioji, Tokyo 192-0397, Japan*

²*Department of Physics, University of Tokyo, Bunkyo-ku, Tokyo 113-0033, Japan*

³*Division of Applied Physics, Faculty of Engineering, Hokkaido University, Sapporo, Hokkaido 060-8628, Japan*

⁴*RIKEN, Center for Emergent Matter Science, Wako Saitama 351-0198, Japan*

(Dated: January 23, 2026)

We propose a framework for generating magnetic structures, inspired by the concept of oriented spin space groups (SSGs): magnetic structures are first generated as totally symmetric representations of an SSG and are then rotated such that they belong to the maximal magnetic space group of the SSG, which we term spin-symmetry-adapted (SSA) structures and oriented SSA structures, respectively. This is a natural framework to enforce fixed magnetic moment magnitudes on the symmetry-equivalent sites as well as to exploit the spin-orbit coupling (SOC)-induced hierarchy of energy scales. To examine the present scheme, we analyze the MAGNDATA database and find that 77% of the reported structures are reproducible at the SSG level, among which 82% are fully reproduced within the oriented SSG scheme, regardless of their spin-only group types or propagation vectors. When the k -index is fixed to its experimental value, the number of magnetic structures generated is on average about nine, also demonstrating the high efficiency of this scheme. Next, to quantitatively assess computational and predictive performance, we perform spin density functional theory calculations for 283 materials, first carrying out self-consistent calculations for SSA structures without SOC, followed by fixed-charge calculations including SOC for the descendant oriented SSA structures. The experimental magnetic structures are reproduced as energetically most stable in 82% of cases at the SSG level without SOC and in 76% of cases at the oriented SSG level with SOC, showing that the fixed-charge scheme enables accurate evaluation of SOC-induced energy differences at low computational cost. The characteristic energy scale among oriented SSA structures is only ~ 0.29 meV per magnetic atom, about 300 times smaller than that of distinct SSA structures, suggesting that calculations with SOC confined to the lowest-energy manifold of oriented SSA structures are sufficient for reliable predictions. These results demonstrate that oriented SSG-based enumeration, combined with the two-step calculations for SSA and oriented SSA structures, provides an efficient and robust route for large-scale magnetic-structure prediction.

I. INTRODUCTION

Spintronics exploits the electron spin degree of freedom in addition to its charge, enabling device concepts with high speed and low power consumption [1, 2]. Most existing spintronic devices rely on ferromagnetic (FM) materials, whereas antiferromagnets (AFMs) have long been considered unsuitable since their nearly vanishing net magnetization complicates detection and control of their magnetic domains. Meanwhile, AFMs offer intrinsic advantages, including negligible stray fields, ultrafast spin dynamics, and robustness against external perturbations [3–7]. In fact, recent experimental advances have demonstrated key functionalities such as tunnel magnetoresistance (TMR) [8–11] and current-induced magnetization or Néel-vector switching [12–29], establishing AFM spintronics as a rapidly expanding research field.

To date, a broad range of AFM materials has been proposed as candidates for spintronic applications. A

prototypical example is the Mn_3X family, in which non-collinear AFM order gives rise to a small but finite canted magnetic moment [30–35]. Despite being antiferromagnetic, these materials possess the same magnetic symmetry as conventional FMs and are therefore compatible with established FM device architectures. More recently, strong interest has turned to *altermagnets* [36–43], a class of collinear AFMs with zero net magnetization in the absence of spin-orbit coupling (SOC), yet exhibiting even-parity spin splitting [37, 44–47]. Beyond these examples, additional symmetry-driven magnetic classes have also been identified, including p -magnets with odd-parity spin splitting [48–51] and q -magnets, which preserve time-reversal symmetry yet exhibit nontrivial responses rooted in nonsymmorphic parent space groups [52, 53]. These systems are predicted to host unconventional phenomena driven by spin ordering, such as TMR effects, without relying on sizable magnetization, thereby substantially broadening the landscape of magnetic materials beyond the conventional FM paradigm.

First-principles calculations have already successfully predicted nontrivial transport phenomena such as the anomalous Hall effect in noncollinear AFMs [54, 55], later confirmed experimentally [30, 32]. Large-scale efforts now aim to determine magnetic ground states using

* tnomoto@tmu.ac.jp; These authors contribute equally to this work.

† kshinohara0508@gmail.com; These authors contribute equally to this work.

high-throughput spin density functional theory (SDFT) calculations, including collinear calculations [56–61] and noncollinear ones [62].

The rapid expansion of magnetic classes and the success of first-principles calculations call for systematic frameworks for predicting magnetic structures. The traditional framework is representation analysis (RA) [63–65], which constructs symmetry-adapted magnetic structures from the irreducible representations (IRs) of the nonmagnetic space group. RA is equivalent and complementary to considering possible magnetic space groups from the nonmagnetic space group [66–68]. A key assumption in RA is that ground-state magnetic structures can be described by a small number of IRs, which is empirically valid in many cases [69].

Although RA has been established as a standard method for magnetic structure analysis and is offered, for example, in ISODISTORT [70] and MAXMAGN [71], it has a limitation. Namely, symmetry-equivalent magnetic atoms in the nonmagnetic structure are not guaranteed to have equal-magnitude magnetic moments in the generated magnetic structures, especially for multi-dimensional IRs. For such multi-dimensional IRs, a linear combination of multiple basis functions is chosen to generate maximal MSGs [71], known as the epikernel or isotropy subgroup [72, 73].

Cluster multipole (CMP) theory is an alternative framework in which magnetic structures are systematically generated and classified according to IRs of the parent point group symmetry [74–76]. This framework will be useful for interpreting the generated magnetic structures and corresponding order parameters. Based on this framework, systematic analyses of databases combined with first-principles calculations have been employed for high-throughput materials prediction [69, 77]. CMP partly resolves the limitation of RA by employing physically motivated vector spherical harmonics as trial basis functions. However, it still suffers from the fundamental limitation of RA mentioned above. As a consequence, exhaustive and efficient enumeration of candidate structures is hindered, motivating the development of alternative formulations.

In parallel, the concept of the spin space group (SSG) has attracted renewed attention as a powerful framework for describing magnetic structures, especially in the context of altermagnets [78–82]. An SSG is defined as a subgroup of the direct product of a parent space group and the $O(3)$ group, in which spatial and spin operations are treated independently [83–88]. Physically, SSGs correspond to the symmetry of magnets in the absence of SOC and therefore encode higher symmetry information than conventional MSGs. As a result, SSGs enable a systematic description of spin correlations that are difficult to analyze within the conventional framework based on RA and MSGs [68, 89]. In addition, as shown in pioneering works on spin-current conductivity [90, 91], comparison between SSGs and MSGs provides a natural way to isolate SOC-induced responses and to assess the

symmetry-allowed magnitude of spin-dependent physical quantities, thereby clarifying various physical phenomena that do not rely on SOC. Recently, the representation theory of SSGs [79, 92–95] and algorithms for deriving symmetry-adapted response tensors [96–98] have been developed.

In this work, we develop an SSG-based algorithm for magnetic-structure generation and perform benchmark analyses of magnetic-structure databases together with first-principles calculations. First, we show that the SSG formulation enables full enumeration of magnetically inequivalent structures up to global $O(3)$ transformations [80–82], which resolves the aforementioned limitation of RA by construction as discussed in Secs. II C and II D. In the following, we refer to these structures as spin-symmetry-adapted (SSA) structures. Second, based on the recently introduced concept of oriented SSG [99], we demonstrate a systematic scheme for enumerating magnetic structures inequivalent up to the parent space group as in conventional MSG classifications, which we term oriented SSA structures. We then apply this framework to the MAGNDATA database [100, 101] and, in combination with high-throughput SDFT calculations, benchmark the predictive performance of AFM structure prediction. A key principle of the proposed scheme is the hierarchy of energy scales between SSA and oriented SSA structures. Because energy differences among oriented SSA structures originate from SOC, they are typically much smaller than those between distinct SSA structures. This hierarchy enables an efficient two-step computational strategy [102]: SDFT calculations without SOC are first used to identify the most stable SSA structure, followed by SOC calculations with fixed charge densities to resolve the oriented SSA structure manifold. We quantitatively assess the validity of this strategy and demonstrate its effectiveness for large-scale magnetic-structure prediction.

The organization of this paper is as follows. In Sec. II, we present an algorithm for magnetic structure generation based on the SSG framework. In Sec. III, we provide a rigorous formulation of the oriented SSG introduced in Ref. [99] and present a method for generating magnetic structures along this concept. In Sec. IV, we apply the proposed algorithm to representative AFM systems and discuss the resulting magnetic structures. In Sec. V, materials listed in the MAGNDATA database are classified according to the oriented SSG scheme, and the range of applicability is discussed. In Sec. VI, we present a benchmark of magnetic structure prediction using high-throughput SDFT calculations. Finally, Sec. VII summarizes our conclusions.

II. ENUMERATING SPIN-SYMMETRY-ADAPTED STRUCTURES

To unambiguously describe our scheme for generating spin-symmetry-adapted (SSA) structures, we first briefly

review terminology and the group structure of spin space groups (SSGs) [86, 103] in Sec. II A. Then, we present a procedure to enumerate SSGs from a space group and a spin-only group in Sec. II B. We describe a generation scheme of commensurate SSA structures from a given space group, a spin-only group, and Wyckoff positions of magnetic sites in Sec. II C. Finally, we discuss practical choices of the space group used in the generation scheme in Sec. II D. Although such a generation scheme with SSG has already been reported, for the zero-propagation vector case in Ref. 80 and for specific applications in Ref. 102, the present self-contained description would be beneficial as it provides a clear and implementable algorithm and explicitly highlights that the SSG-based generation guarantees identical magnitudes of magnetic moments for sites belonging to the same Wyckoff position.

A. Group structure of spin space group

Let \mathcal{X} be a subgroup of the direct product of the Euclidean group $E(3)$ and the three-dimensional orthogonal group $O(3)$. If the following $\mathcal{G}(\mathcal{X})$ is a space group, \mathcal{X} is called a spin space group (SSG),

$$\mathcal{G}(\mathcal{X}) = \{g \in E(3) \mid \exists \mathbf{U} \in O(3) \text{ s.t. } (g, \mathbf{U}) \in \mathcal{X}\}. \quad (1)$$

For a spin space group \mathcal{X} , we call $\mathcal{G}(\mathcal{X})$ a family space group of \mathcal{X} . A maximal space subgroup of a spin space group \mathcal{X} is defined as

$$\mathcal{H}(\mathcal{X}) = \{g \in E(3) \mid (g, \mathbf{I}) \in \mathcal{X}\}, \quad (2)$$

where \mathbf{I} is the identity rotation in $O(3)$. The maximal space subgroup $\mathcal{H}(\mathcal{X})$ is a normal subgroup of $\mathcal{G}(\mathcal{X})$.

A family spin point group of spin space group \mathcal{X} is defined as

$$\mathcal{B}(\mathcal{X}) = \{\mathbf{U} \in O(3) \mid \exists g \in E(3) \text{ s.t. } (g, \mathbf{U}) \in \mathcal{X}\}. \quad (3)$$

A spin-only group of spin space group \mathcal{X} is defined as

$$\mathcal{B}_{\text{so}}(\mathcal{X}) = \{\mathbf{U} \in O(3) \mid ((\mathbf{I}, \mathbf{0}), \mathbf{U}) \in \mathcal{X}\}. \quad (4)$$

The spin-only group $\mathcal{B}_{\text{so}}(\mathcal{X})$ is a normal subgroup of $\mathcal{B}(\mathcal{X})$. The direct product group $\mathcal{H}(\mathcal{X}) \times \mathcal{B}_{\text{so}}(\mathcal{X})$ is a normal subgroup of \mathcal{X} .

From Goursat's lemma [86, 104], there is a group isomorphism between the quotient groups

$$\mathcal{X}/(\mathcal{H}(\mathcal{X}) \times \mathcal{B}_{\text{so}}(\mathcal{X})) \cong \mathcal{G}(\mathcal{X})/\mathcal{H}(\mathcal{X}) \cong \mathcal{B}(\mathcal{X})/\mathcal{B}_{\text{so}}(\mathcal{X}), \quad (5)$$

where we let $U : \mathcal{G}(\mathcal{X})/\mathcal{H}(\mathcal{X}) \rightarrow \mathcal{B}(\mathcal{X})/\mathcal{B}_{\text{so}}(\mathcal{X})$ be the isomorphism. Then, spin space group \mathcal{X} is uniquely characterized by the triplet $(\mathcal{H}(\mathcal{X}), \mathcal{B}_{\text{so}}(\mathcal{X}), U)$.

From Hermann's theorem [105], there exists a unique group $\mathcal{M}(\mathcal{X})$ satisfying the following two conditions: (1) $\mathcal{M}(\mathcal{X})$ is a translationengleiche subgroup (t-subgroup)

of $\mathcal{G}(\mathcal{X})$, where their translation subgroups are identical; (2) $\mathcal{H}(\mathcal{X})$ is a klassengleiche subgroup (k-subgroup) of $\mathcal{M}(\mathcal{X})$, where their point groups are identical. Here, $\mathcal{H}(\mathcal{X})$ is a normal subgroup of $\mathcal{M}(\mathcal{X})$ because $\mathcal{H}(\mathcal{X}) \trianglelefteq \mathcal{G}(\mathcal{X})$ and $\mathcal{M}(\mathcal{X}) \leq \mathcal{G}(\mathcal{X})$. Also, $\mathcal{M}(\mathcal{X})$ is a normal subgroup of $\mathcal{G}(\mathcal{X})$ because $\mathcal{M}(\mathcal{X})$ is uniquely defined as a subgroup of $\mathcal{G}(\mathcal{X})$ with the above two conditions.

B. Enumeration of spin space groups from family space group and spin-only group

Conversely, the group isomorphism in Eq. (5) provides a systematic way to enumerate spin space groups \mathcal{X} from a given space group \mathcal{G} and spin-only group \mathcal{B}_{so} . For every normal space subgroup \mathcal{H} of \mathcal{G} , if there exists an injective homomorphism $U : \mathcal{G}/\mathcal{H} \rightarrow O(3)/\mathcal{B}_{\text{so}}(\mathcal{X})$, then the triplet $(\mathcal{H}, \mathcal{B}_{\text{so}}, U)$ uniquely determines a spin space group. For later convenience, we denote a translation subgroup of \mathcal{G} as

$$\mathcal{T}(\mathcal{G}) = \{(\mathbf{I}, \mathbf{t}) \mid (\mathbf{I}, \mathbf{t}) \in \mathcal{G}\}, \quad (6)$$

and the coset decomposition of \mathcal{G} by $\mathcal{T}(\mathcal{G})$ as

$$\mathcal{G} = \bigcup_{i=1}^n g_i \mathcal{T}(\mathcal{G}), \quad (7)$$

where $n = |\mathcal{G} : \mathcal{T}(\mathcal{G})|$, and $g_i = (\mathbf{R}_i, \boldsymbol{\tau}_i)$ are representatives of cosets.

When a spin space group is a stabilizer of a magnetic structure, its spin-only group \mathcal{B}_{so} is classified into four types up to transformations [86]: nonmagnetic ($\mathcal{B}_{\text{so}} \cong O(3)$), collinear ($\mathcal{B}_{\text{so}} \cong \mathbb{Z}_2 \ltimes SO(2)$), coplanar ($\mathcal{B}_{\text{so}} \cong \mathbb{Z}_2$), and noncoplanar ($\mathcal{B}_{\text{so}} \cong 1$). For nonmagnetic cases, all enumerated spin space groups are a direct product of a normal space subgroup of \mathcal{G} and $O(3)$. As this is trivial, we henceforth focus on collinear, coplanar, and noncoplanar spin-only groups.

A spin-structure dimension d is defined as the dimension of the vector space spanned by magnetic moments [106]; $d = 1, 2, 3$ correspond to collinear, coplanar, and noncoplanar spin-only groups, respectively. The dimension of $\mathcal{B}(\mathcal{X})/\mathcal{B}_{\text{so}}(\mathcal{X})$ is equal to the spin-structure dimension d .

Because there are infinitely many space subgroups for a given space group \mathcal{G} , we first consider the intermediate space group \mathcal{M} between \mathcal{G} and \mathcal{H} such that (1) \mathcal{M} is a normal t-subgroup of \mathcal{G} and (2) \mathcal{H} is a normal k-subgroup of \mathcal{M} with a given index of $N_k = |\mathcal{M} : \mathcal{H}|$. We call N_k the k-index, which corresponds to how many times a magnetic unit cell is enlarged compared to the original unit cell. There are only a finite number of t-subgroups \mathcal{M} for a given space group \mathcal{G} .

Therefore, inputs $(\mathcal{G}, \mathcal{B}_{\text{so}}, N_k)$ give a finite number of spin space groups \mathcal{X} with family space group $\mathcal{G}(\mathcal{X}) = \mathcal{G}$ and spin-only group $\mathcal{B}_{\text{so}}(\mathcal{X}) = \mathcal{B}_{\text{so}}$. A resulting spin space

group \mathcal{X} and associated groups can be expressed as

$$\mathcal{M} = \bigcup_{m=1}^{N_k} (\mathbf{I}, \mathbf{t}_m) \mathcal{H} \quad (8)$$

$$\mathcal{G} = \bigcup_{I=1}^{N_t} g_{i_I} \mathcal{M} \quad (9)$$

$$\mathcal{X} = \bigcup_{I=1}^{N_t} \bigcup_{m=1}^{N_k} (g_{i_I}(\mathbf{I}, \mathbf{t}_m), \mathbf{U}_{Im}) (\mathcal{H} \times \mathcal{B}_{\text{so}}), \quad (10)$$

where $N_t = |\mathcal{G} : \mathcal{M}|$, $\{i_1, \dots, i_{N_t}\} \subseteq \{1, \dots, n\}$, and $\{(\mathbf{I}, \mathbf{t}_m)\}$ and $\{g_{i_I}\}$ are coset representatives of \mathcal{M}/\mathcal{H} and \mathcal{G}/\mathcal{M} , respectively. The spin rotation \mathbf{U}_{Im} is arbitrarily chosen from a coset $U(g_{i_I}(\mathbf{I}, \mathbf{t}_m)\mathcal{H})$.

We consider representative spin space groups up to transformations in $\mathcal{G} \times O(3)$. Thus, we identify two spin space groups \mathcal{X}_1 and \mathcal{X}_2 constructed from the same triplet $(\mathcal{H}, \mathcal{B}_{\text{so}}, U)$ if there exists $(g, \mathbf{U}) \in \mathcal{G} \times O(3)$ such that

$$(g, \mathbf{U})^{-1} \mathcal{X}_1 (g, \mathbf{U}) = \mathcal{X}_2. \quad (11)$$

By this definition, we choose \mathcal{B}_{so} with a rotation parallel to the z -axis for collinear cases, and a reflection perpendicular to the z -axis for coplanar cases, without loss of generality.

Note that these conjugacy classes of spin space groups are different from their isomorphism classes. The latter considers equivalence up to transformations in $\mathcal{N}(\mathcal{G}) \times O(3)$, where $\mathcal{N}(\mathcal{G})$ is the affine normalizer of \mathcal{G} in $E(3)$. We choose the former equivalence because it is suitable for exhaustively generating candidate magnetic structures. For example, each axis of an orthorhombic space group is taken as inequivalent under the former equivalence, and magnetic structures polarized along each axis can be generated separately.

A detailed algorithm to enumerate spin space groups in Eq. (10) up to transformations in $\mathcal{G} \times O(3)$ is provided in Appendix A.

C. Generation of spin-symmetry-adapted structures from spin space group

For a given family space group \mathcal{G} , a spin-only group \mathcal{B}_{so} , and k -index N_k , we first enumerate spin space groups \mathcal{X} using the procedure in Sec. II B. By construction, each Wyckoff position of \mathcal{G} belongs to a single orbit of \mathcal{X} because a symmetry operation in \mathcal{G} has a one-to-one correspondence to that in \mathcal{X} through Eq. (10). Thus, magnetic sites belonging to the same Wyckoff position of \mathcal{G} have identical magnitudes of magnetic moments in a magnetic structure stabilized by \mathcal{X} .

We next consider the action of spin symmetry operations in \mathcal{X} on magnetic moments of a magnetic structure. We denote the κ th magnetic site in the ℓ th unit cell as $\mathbf{r}(\ell\kappa)$, where $\kappa \in \{1, \dots, m\}$ and $\ell \in \mathbb{Z}^3$. We write the magnetic moment at the site $\mathbf{r}(\ell\kappa)$ as $\mathbf{m}_{\mathbf{r}(\ell\kappa)}$. For a spin

symmetry operation $(g, \mathbf{U}) \in \mathcal{X}$, its action on the magnetic moments \mathbf{m} is defined as

$$[(g, \mathbf{U})\mathbf{m}]_{\mathbf{r}(\ell\kappa)} = \mathbf{U} \mathbf{m}_{g^{-1}\mathbf{r}(\ell\kappa)}. \quad (12)$$

This action provides a representation matrix of \mathcal{X} on the magnetic moments as

$$\begin{aligned} & [(g, \mathbf{U})\mathbf{m}]_{r_\mu(\ell\kappa)} \\ &= \sum_{\ell' \in \mathbb{Z}^3} \sum_{\kappa'=1}^m \sum_{\mu'=1}^3 \Gamma_{\ell\kappa\mu; \ell'\kappa'\mu'}((g, \mathbf{U})) \mathbf{m}_{\mathbf{r}_{\mu'}(\ell'\kappa')}, \end{aligned} \quad (13)$$

where $r_\mu(\ell\kappa)$ is the μ th component of $\mathbf{r}(\ell\kappa)$, and the representation matrix is given by

$$\Gamma_{\ell\kappa; \ell'\kappa'}^{\text{site}}(g) = \delta_{\mathbf{r}(\ell\kappa), \mathbf{r}(\ell'\kappa')} \quad (14)$$

$$\Gamma_{\ell\kappa\mu; \ell'\kappa'\mu'}((g, \mathbf{U})) = \Gamma_{\ell\kappa; \ell'\kappa'}^{\text{site}}(g) [\mathbf{U}]_{\mu\mu'}. \quad (15)$$

When the spin symmetry operation can be viewed as a magnetic symmetry operation with $(\det \mathbf{R}_g) \mathbf{R}_g = (\det \mathbf{U}) \mathbf{U}$ [103], the above representation matrices are identical to those for magnetic space groups in Ref. 107, where we denote the rotation part of g as \mathbf{R}_g .

Symmetry-adapted magnetic moments $\mathbf{m}^{(\alpha)}$ of \mathcal{X} are invariant under all spin symmetry operations in \mathcal{X} ,

$$(g, \mathbf{U})\mathbf{m}^{(\alpha)} = \mathbf{m}^{(\alpha)}. \quad (16)$$

We formally refer to a magnetic structure with $\mathbf{m}^{(\alpha)}$ as a spin-symmetry-adapted (SSA) structure of \mathcal{X} . As shown in Appendix B, such symmetry-adapted magnetic moments can be obtained by applying the projection operator of \mathcal{X} . If multiple $p_{\mathcal{X}} (> 1)$ linearly independent symmetry-adapted magnetic moments exist, we label them as $\mathbf{m}^{(\alpha=1)}, \dots, \mathbf{m}^{(\alpha=p_{\mathcal{X}})}$.

D. Practical choices of family space group

For a given nonmagnetic structure, the natural first choice of the family space group in Sec. II C is its space group \mathcal{G}_0 . However, a combination of \mathcal{G}_0 and a specified spin-only group \mathcal{B}_{so} may admit only the trivial solution in Eq. (16), yielding no nonzero symmetry-adapted magnetic moments. When this occurs, we consider its maximal t-subgroups \mathcal{G}'_0 that preserve the multiplicities [108] of the given Wyckoff positions of magnetic sites, and use \mathcal{G}'_0 as the family space group. This procedure is repeated until we obtain nonzero symmetry-adapted magnetic moments. Because the given Wyckoff positions are not split in \mathcal{G}'_0 , the resulting symmetry-adapted magnetic moments have identical magnitudes for magnetic sites in the same given Wyckoff position.

III. ENUMERATING SYMMETRY-ADAPTED MAGNETIC STRUCTURES BY SUBDuing SSG TO MSG

Until now, we have discussed SSGs up to $O(3)$ transformations in the spin space, and the spin axis of a re-

sulting symmetry-adapted magnetic structure is not fixed in general. However, in many cases, the spin axes are aligned along specific crystallographic directions or high-symmetry directions due to SOC. To describe such situations, we here present a systematic procedure to enumerate SSGs with maximal magnetic space group correspondences from a given SSG. We call such enumerated SSGs oriented spin space groups (oriented SSGs) hereafter, following Ref. 99, and use them to describe both a SSG and a magnetic space group (MSG) of a magnetic structure simultaneously.

We define a family point group of \mathcal{X} as

$$\mathcal{P}(\mathcal{X}) = \{\mathbf{R} \mid ((\mathbf{R}, \boldsymbol{\tau}), \mathbf{U}) \in \mathcal{X}\}. \quad (17)$$

We call \mathcal{X} triclinic if $\mathcal{P}(\mathcal{X}) = 1$ or $\bar{1}$. When \mathcal{X} is triclinic, there is no restriction on spin axes. Thus, we assume \mathcal{X} is not triclinic in what follows.

We denote the time-reversal operation as θ and set

$$\theta_s = \begin{cases} 1 & (s = 1), \\ \theta & (s = -1). \end{cases} \quad (18)$$

We write a MSG induced from \mathcal{X} with spin transformation $\mathbf{Q} \in O(3)$ as

$$\begin{aligned} \mathcal{M}(\mathcal{X}, \mathbf{Q}) \\ = \left\{ (\mathbf{R}, \boldsymbol{\tau}) \theta_{\det \mathbf{U}} \mid \begin{array}{l} ((\mathbf{R}, \boldsymbol{\tau}), \mathbf{U}) \in \mathcal{X}, \\ (\det \mathbf{R}) \mathbf{R} = (\det \mathbf{U}) \mathbf{Q}^{-1} \mathbf{U} \mathbf{Q} \end{array} \right\}, \end{aligned} \quad (19)$$

where spin operation $((\mathbf{R}, \boldsymbol{\tau}), \mathbf{U})$ is mapped to a magnetic operation if $(\det \mathbf{R}) \mathbf{R} = (\det \mathbf{U}) \mathbf{U}$ [103].

In this paper, we define an oriented SSG of \mathcal{X} as a pair $(\mathcal{X}, \mathbf{Q})$ with equivalence relation $(\mathcal{X}, \mathbf{Q}) \sim (\mathcal{X}, \mathbf{Q}')$ if $\mathcal{M}(\mathcal{X}, \mathbf{Q})$ and $\mathcal{M}(\mathcal{X}, \mathbf{Q}')$ are conjugate by certain $g \in \mathcal{G}(\mathcal{X})$. Furthermore, we only consider oriented SSGs such that $\mathcal{M}(\mathcal{X}, \mathbf{Q})$ is maximal among all MSGs induced from \mathcal{X} by varying $\mathbf{Q} \in O(3)$.

A. Noncoplanar oriented spin space group

First, we consider a noncoplanar SSG \mathcal{X} with $\mathcal{B}_{\text{so}}(\mathcal{X}) = 1$. For a subgroup \mathcal{Y} of \mathcal{X} with $\mathcal{Y} \supseteq \mathcal{T}(\mathcal{H}(\mathcal{X}))$, \mathcal{Y} and $\mathcal{M}(\mathcal{Y}, \mathbf{Q})$ have a one-to-one correspondence for some $\mathbf{Q} \in O(3)$ if $(\det \mathbf{R}) \mathbf{R} = (\det \mathbf{U}) \mathbf{Q}^{-1} \mathbf{U} \mathbf{Q}$ for all $((\mathbf{R}, \boldsymbol{\tau}), \mathbf{U}) \in \mathcal{Y}$. This condition can be seen as an equivalence of two orthogonal representations of $\mathcal{Y}/\mathcal{T}(\mathcal{H}(\mathcal{X}))$,

$$\begin{aligned} \Gamma_r : \mathcal{Y}/\mathcal{T}(\mathcal{H}(\mathcal{X})) &\rightarrow SO(3); \\ ((\mathbf{R}, \boldsymbol{\tau}), \mathbf{U}') \mathcal{T}(\mathcal{H}(\mathcal{X})) &\mapsto (\det \mathbf{R}) \mathbf{R}, \end{aligned} \quad (20)$$

$$\begin{aligned} \Gamma_s : \mathcal{Y}/\mathcal{T}(\mathcal{H}(\mathcal{X})) &\rightarrow SO(3); \\ ((\mathbf{R}, \boldsymbol{\tau}), \mathbf{U}') \mathcal{T}(\mathcal{H}(\mathcal{X})) &\mapsto (\det \mathbf{U}') \mathbf{U}'. \end{aligned} \quad (21)$$

If there exists a real intertwiner $\mathbf{Q}_* \in O(3)$ between Γ_r and Γ_s , SSG \mathcal{Y} can be identified with a MSG

$$\mathcal{M}(\mathcal{Y}, \mathbf{Q}_*) = \{(\mathbf{R}, \boldsymbol{\tau}) \theta_{\det \mathbf{U}} \mid ((\mathbf{R}, \boldsymbol{\tau}), \mathbf{U}) \in \mathcal{Y}\}. \quad (22)$$

Such a real intertwiner can be numerically constructed by the algorithm described in Appendix C, if it exists. Thus, by enumerating subgroups of $\mathcal{X}/\mathcal{T}(\mathcal{H}(\mathcal{X}))$ and finding a real intertwiner between Γ_r and Γ_s for each subgroup, we can enumerate inequivalent MSGs induced from \mathcal{X} . We further filter the enumerated MSGs to keep only those with maximal symmetry, which correspond to a finite number of oriented SSGs.

B. Collinear oriented spin space group

For a collinear SSG \mathcal{X} , if its family point group and a normalizer of its spin-only group intersect trivially as $\mathcal{P}(\mathcal{X}) \cap \mathcal{N}(\mathcal{B}_{\text{so}}) = 1$, no nontrivial rotation symmetry operation survives in the induced MSG for any $\mathbf{Q} \in O(3)$, which implies triclinic MSG. Because there is no restriction on spin axes in triclinic MSGs, we enumerate candidate spin axes for oriented spin-only groups from $\mathbf{R} \in \mathcal{P}(\mathcal{X}) \setminus \{\mathbf{I}, -\mathbf{I}\}$ in what follows. We denote a transformation to align with a candidate spin axis as $\mathbf{Q}' \in SO(3)$ and a transformed SSG of \mathcal{X} by \mathbf{Q}' as \mathcal{X}' . For notational simplicity, we assume the spin axis of $\mathcal{B}_{\text{so}}(\mathcal{X}')$ is along the z -axis in what follows.

For $((\mathbf{R}, \boldsymbol{\tau}), \mathbf{U}') \in \mathcal{X}'$, we decompose spatial and spin rotation into two-dimensional rotations around the z -axis and a sign flip along the z -axis, if possible:

$$\mathbf{R}_{xy} \oplus p_z = \mathbf{R} \quad (\mathbf{R}_{xy} \in O_{xy}(2), p_z \in \mathbb{Z}_2) \quad (23)$$

$$\mathbf{U}'_{xy} \oplus u'_z = \mathbf{U}' \quad (\mathbf{U}'_{xy} \in O_{xy}(2), u'_z \in \mathbb{Z}_2), \quad (24)$$

where $O_{xy}(2)$ is a two-dimensional orthogonal group acting on the xy -plane. Because $\mathcal{B}_{\text{so}} = O_{xy}(2) \oplus 1$ and $\mathcal{N}(\mathcal{B}_{\text{so}})/\mathcal{B}_{\text{so}} = 1 \oplus \mathbb{Z}_2$, a transformation $\mathbf{Q} \in \mathcal{N}(\mathcal{B}_{\text{so}})$ acts on $\mathcal{N}(\mathcal{B}_{\text{so}})/\mathcal{B}_{\text{so}}$ as identity. Thus, every $\mathbf{Q} \in \mathcal{N}(\mathcal{B}_{\text{so}})$ gives the same MSG $\mathcal{M}(\mathcal{X}', \mathbf{Q})$ and we do not need to enumerate \mathbf{Q} further. We directly filter the enumerated MSGs $\mathcal{M}(\mathcal{X}', \mathbf{Q}')$ for each candidate spin axis to keep only those with maximal symmetry, which correspond to a finite number of oriented SSGs.

C. Coplanar oriented spin space group

For a coplanar SSG \mathcal{X} , it suffices to enumerate candidate spin axes only from $\mathbf{R} \in \mathcal{P}(\mathcal{X}) \setminus \{\mathbf{I}, -\mathbf{I}\}$ as in the collinear case. We denote a transformation to align with a candidate spin axis as $\mathbf{Q}' \in SO(3)$ and a transformed SSG of \mathcal{X} by \mathbf{Q}' as \mathcal{X}' . For notational simplicity, we assume the spin axis of $\mathcal{B}_{\text{so}}(\mathcal{X}')$ is along the z -axis in what follows.

We decompose spatial and spin rotation parts of spin symmetry operations of \mathcal{X}' as in Eqs. (23) and (24) if possible. We denote by \mathcal{Y}' a subgroup of \mathcal{X}' such that all spin symmetry operations are decomposed as above:

$$\mathcal{Y}' = \bigcup_j ((\mathbf{R}_j, \boldsymbol{\tau}_j), \mathbf{U}'_j) (\mathcal{T}(\mathcal{H}(\mathcal{X}')) \times \mathcal{B}_{\text{so}}(\mathcal{X}')). \quad (25)$$

To enumerate MSGs induced from subgroups of \mathcal{Y}' , we use the fact that a MSG has a one-to-one correspondence to a pair of its family space group \mathcal{G}' and maximal space subgroup \mathcal{H}' [109] as follows. We first enumerate subgroups \mathcal{G}' of $\mathcal{G}(\mathcal{Y}')$ with $\mathcal{G}' \supseteq \mathcal{T}(\mathcal{H}(\mathcal{X}'))$. For each \mathcal{G}' , we further enumerate its normal subgroups $\mathcal{H}' \trianglelefteq \mathcal{G}'$ with $|\mathcal{G}'/\mathcal{H}'| \leq 2$. For a pair of $(\mathcal{G}', \mathcal{H}')$, we assign a spin rotation for coset representative (\mathbf{R}_j, τ_j) from $\mathbf{U}'_j \mathcal{B}_{\text{so}}(\mathcal{X}')$ such that \mathcal{H}' corresponds to identity and $\mathcal{G}' \setminus \mathcal{H}'$ corresponds to time-reversal operations:

$$\mathbf{V}'_j = \begin{cases} \mathbf{U}'_j & ((\mathbf{R}_j, \tau_j) \in \mathcal{H}', \det \mathbf{U}'_j = 1) \\ \mathbf{U}'_j \boldsymbol{\sigma}_z & ((\mathbf{R}_j, \tau_j) \in \mathcal{H}', \det \mathbf{U}'_j = -1) \\ \mathbf{U}'_j \boldsymbol{\sigma}_z & ((\mathbf{R}_j, \tau_j) \in \mathcal{G}' \setminus \mathcal{H}', \det \mathbf{U}'_j = 1) \\ \mathbf{U}'_j & ((\mathbf{R}_j, \tau_j) \in \mathcal{G}' \setminus \mathcal{H}', \det \mathbf{U}'_j = -1) \end{cases}, \quad (26)$$

where $\boldsymbol{\sigma}_z \in \mathcal{B}_{\text{so}}(\mathcal{X}')$ is a mirror operation perpendicular to the z -axis, and is used to adjust the determinant of spin rotations. The pair $(\mathcal{G}', \mathcal{H}')$ with assigned spin rotations $\{\mathbf{V}'_j\}$ has a one-to-one correspondence to a MSG if $(\det \mathbf{R}_j) \mathbf{R}_j = (\det \mathbf{V}'_j) \mathbf{Q}^{-1} \mathbf{V}'_j \mathbf{Q}$ for all $(\mathbf{R}_j, \tau_j) \mathcal{T}(\mathcal{H}(\mathcal{X}')) \in \mathcal{G}' / \mathcal{T}(\mathcal{H}(\mathcal{X}'))$ with a certain $\mathbf{Q} \in O(3)$.

Because \mathbf{R}_j and \mathbf{V}'_j are decomposed into two-dimensional rotations around z -axis and a sign-flip along z -axis as

$$\mathbf{R}_{j,xy} \oplus p_{j,z} = \mathbf{R}_j \quad (\mathbf{R}_{j,xy} \in O_{xy}(2), p_{j,z} \in \mathbb{Z}_2) \quad (27)$$

$$\mathbf{V}'_{j,xy} \oplus v'_{j,z} = \mathbf{V}'_j \quad (\mathbf{V}'_{j,xy} \in O_{xy}(2), v'_{j,z} \in \mathbb{Z}_2), \quad (28)$$

the above condition requires the equivalence of (z, z) -components

$$(\det \mathbf{R}_j) p_{j,z} = (\det \mathbf{V}'_j) v'_{j,z} \quad (29)$$

for all $(\mathbf{R}_j, \tau_j) \mathcal{T}(\mathcal{H}(\mathcal{X}')) \in \mathcal{G}' / \mathcal{T}(\mathcal{H}(\mathcal{X}'))$. In addition, the following two-dimensional representations must be equivalent:

$$\begin{aligned} \Gamma_{r,xy} : \mathcal{G}' / \mathcal{T}(\mathcal{H}(\mathcal{X}')) &\rightarrow O_{xy}(2); \\ (\mathbf{R}_j, \tau_j) \mathcal{T}(\mathcal{H}(\mathcal{X}')) &\mapsto (\det \mathbf{R}_j) \mathbf{R}_{j,xy}, \end{aligned} \quad (30)$$

$$\begin{aligned} \Gamma_{s,xy} : \mathcal{G}' / \mathcal{T}(\mathcal{H}(\mathcal{X}')) &\rightarrow O_{xy}(2); \\ (\mathbf{R}_j, \tau_j) \mathcal{T}(\mathcal{H}(\mathcal{X}')) &\mapsto (\det \mathbf{V}'_j) \mathbf{V}'_{j,xy}. \end{aligned} \quad (31)$$

An intertwiner $\mathbf{Q}_{xy} \in O_{xy}(2)$ between $\Gamma_{r,xy}$ and $\Gamma_{s,xy}$ can be constructed as shown in Appendix C, if it exists. Thus, by enumerating pairs of $(\mathcal{G}', \mathcal{H}')$ with Eq. (29) and finding a real intertwiner between $\Gamma_{r,xy}$ and $\Gamma_{s,xy}$, we can enumerate inequivalent MSGs induced from \mathcal{X}' . We further filter the enumerated MSGs to keep only those with maximal symmetry, which correspond to a finite number of oriented SSGs.

D. Chirality of spin space group

So far, the transformation \mathbf{Q} between SSGs has been considered in $O(3)$. However, we should care about the

parity of \mathbf{Q} when discussing chirality of coplanar magnetic structures. Motivated by the definition of spatial chirality [110], we say that an object is spin-chiral if it cannot be superimposed on its time-reversed counterpart by a proper spin rotation. Conversely, if such a mapping exists, we call the object spin-achiral. For SSGs, this definition is rephrased as follows: a SSG \mathcal{X} is spin-chiral if \mathcal{X} and $(1, \bar{1})^{-1} \mathcal{X}(1, \bar{1})$ are not equivalent by any spin transformation $\mathbf{Q} \in SO(3)$. However, as $(1, \bar{1})^{-1}(g, \mathbf{U})(1, \bar{1}) = (g, \mathbf{U})$ for all $(g, \mathbf{U}) \in \mathcal{X}$, they are always equivalent by any $\mathbf{Q} \in O(3)$. Thus, a SSG is always spin-achiral.

That being said, there are still discussions on chirality for coplanar magnetic structures with SOC [111–113]. Vector spin chirality is commonly used to capture such chirality as an ad hoc indicator [114, 115]. Thus, we further consider chirality of SSGs by restricting spin transformations \mathbf{Q} to $SO(d) \oplus \mathbf{I}_{3-d}$ with spin-structure dimension $d = 1, 2$. We refer to such chirality for collinear ($d = 1$) and coplanar ($d = 2$) objects as spin-axichirality and spin-planochirality, respectively. The terms “axichirality” and “planochirality” are borrowed from the corresponding concept in spatial chirality [116, 117]. No collinear SSG is spin-axichiral because $O(1)$ is abelian. Thus, we focus on spin-planochirality and provide a procedure to judge spin-planochirality of coplanar SSGs in Appendix D. For a spin-planochiral coplanar SSG \mathcal{X} , we generate oriented SSGs from both \mathcal{X} and its “enantiomorph” SSG up to orientation-preserving spin transformation in $SO(2) \oplus 1$.

IV. REPRESENTATIVE EXAMPLES

We apply and demonstrate the present enumeration scheme to three representative magnetic structures: collinear MnTe in Sec. IV A, coplanar Mn₃Sn in Sec. IV B, and noncoplanar CoTa₃S₆ in Sec. IV C.

A. Collinear MnTe

The magnetic structure of MnTe reported in Ref. 118 is assigned to MSG *Cmem* (BNS No. 63.457) and collected in entry #0.800 of MAGNCDATA [100]. Its family space group is *P6₃/mmc* (No. 194) and the magnetic Mn atoms are located at Wyckoff position *2a*. Its magnetic structure is collinear within the *ab* plane. The magnetic unit cell is the same as the nonmagnetic one.

Figure 1 (a) illustrates the enumeration procedure for collinear SSGs of MnTe with $N_k = 1$. Because the magnetic unit cell coincides with the nonmagnetic one, only SSGs with $N_k = 1$ are considered. Under this constraint, two collinear SSGs compatible with the family space group $\mathcal{G} = P6_3/mmc$ are obtained: SSG-1, which yields an antiferromagnetic order, and SSG-2, which yields a ferromagnetic order. Although the illustrative SSA structures are drawn with magnetic moments along the *c*-axis,

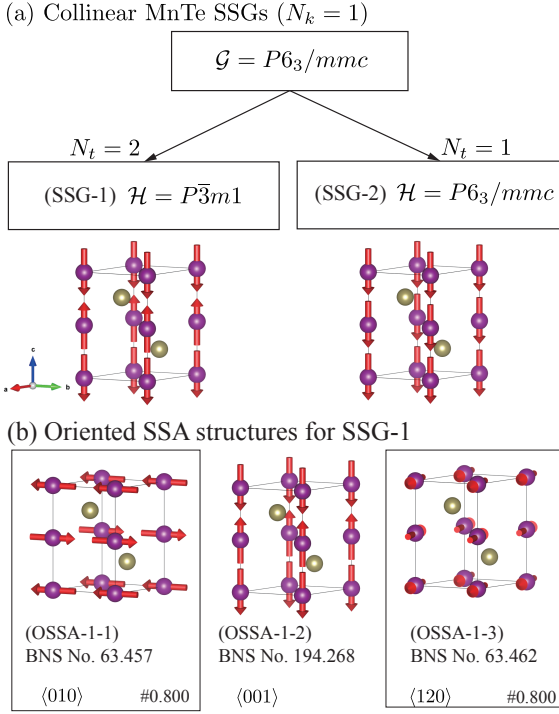


FIG. 1. Enumeration of collinear magnetic structures of MnTe. (a) SSGs compatible with the nonmagnetic family space group $\mathcal{G} = P6_3/mmc$ (No. 194), collinear, and $N_k = 1$. Two SSGs are obtained: SSG-1 with normal space subgroup $\mathcal{H} = P\bar{3}m1$ (No. 164), and SSG-2 with $\mathcal{H} = P6_3/mmc$ (No. 194). For each SSG, its SSA structure is shown beneath the corresponding box. (b) Collinear oriented SSA structures derived from SSG-1. Three distinct oriented SSA structures, OSSA-1-1, OSSA-1-2, and OSSA-1-3, are obtained, corresponding to magnetic moments oriented along the crystallographic directions $\langle 010 \rangle$, $\langle 001 \rangle$, and $\langle 120 \rangle$, respectively. Each magnetic space-group type of the oriented SSA structures is indicated by the BNS numbers [119]. The magnetic moments lying in the ab plane (OSSA-1-1 and OSSA-1-3) are consistent with the experimentally reported one (#0.800 in MAGNDATA).

the SSG alone does not fix the absolute direction of the magnetic moments.

To resolve the magnetic moment directions, we further derive oriented SSA structures from SSG-1 as illustrated in Fig. 1 (b). This generates three inequivalent collinear oriented SSA structures corresponding to distinct crystallographic directions. Two of them place the magnetic moments in the ab plane, in agreement with the experimentally reported magnetic structure of MnTe.

B. Coplanar Mn_3Sn

Two magnetic structures of Mn_3Sn are collected in entries #0.199 and #0.200 of MAGNDATA [100], re-

ported in Ref. 120. They are assigned to MSGs $Cmc'm'$ (BNS No. 63.463) and $Cm'cm'$ (BNS No. 63.464), respectively. Their family space group is $P6_3/mmc$ (No. 194) and the magnetic Mn atoms are located at Wyckoff position $6h$. Their magnetic structures are coplanar within the ab plane. The magnetic unit cell is the same as the nonmagnetic one, $N_k = 1$.

Figure 2 (a) illustrates the enumeration procedure for coplanar SSGs of Mn_3Sn with $N_k = 1$. Because the magnetic unit cell coincides with the nonmagnetic one, only SSGs with $N_k = 1$ are considered. Under this constraint, five coplanar SSGs compatible with the family space group $\mathcal{G} = P6_3/mmc$ are obtained: SSG-1 to SSG-5. Although SSG-3 and SSG-4 are enumerated from the same normal space subgroup $\mathcal{H} = P\bar{6}m2$, their spin rotation parts are inequivalent. SSG-1 and SSG-2 yield one-dimensional symmetry-adapted magnetic moments, respectively. SSG-3 to SSG-5 yield two-dimensional symmetry-adapted magnetic moments with collinear-like bases.

We further derive oriented SSA structures from SSG-2 as illustrated in Fig. 2 (b). Because SSG-2 is spin-planochiral, we generate oriented SSA structures from both SSG-2 and its enantiomeric one as discussed in Sec. III D. Three distinct crystallographic orientations for coplanar spin-only groups are obtained, $\langle 001 \rangle$, $\langle 010 \rangle$, and $\langle 120 \rangle$. For $\langle 001 \rangle$, four oriented SSA structures are generated, OSSA-2-1 to OSSA-2-4. OSSA-2-3 and OSSA-2-4 correspond to the experimentally reported magnetic structures of Mn_3Sn in entries #0.199 and #0.200 of MAGNDATA, respectively. While OSSA-2-3 and OSSA-2-4 are often referred to as inverse-triangular, they are equivalent to normal triangular OSSA-2-2 and OSSA-2-1, respectively, by a global spin transformation $C_{6z}C_{2x}$. Therefore, the distinction by spin-planochirality should be used for coplanar Mn_3Sn when we discuss these magnetic structures. For $\langle 010 \rangle$ and $\langle 120 \rangle$, two oriented SSA structures are generated for each orientation. Because the enantiomeric SSG yields isomorphic oriented SSGs in these cases, the spin-planochirality does not affect the resulting oriented SSA structures.

C. Noncoplanar CoTa_3S_6

The magnetic structure of CoTa_3S_6 reported in Ref. 121 is assigned to MSG $P32'1$ (BNS No. 150.27) and collected in entry #3.25 of MAGNDATA [100]. Its family space group is $P6_322$ (No. 182) and the magnetic Co atoms are located at Wyckoff position $2d$. Its magnetic structure is noncoplanar, and the magnetic unit cell is four times larger than the nonmagnetic one, $N_k = 4$.

Figure 3 illustrates the enumeration procedure for noncoplanar SSGs of CoTa_3S_6 with $N_k = 4$. Under this constraint, six noncoplanar SSGs compatible with the family space group $\mathcal{G} = P6_322$ are obtained: SSG-1 to SSG-6. Although SSG-3 to SSG-6 are enumerated from the same normal space subgroup $\mathcal{H} = P3$ with $1 \times 1 \times 4$ magnetic

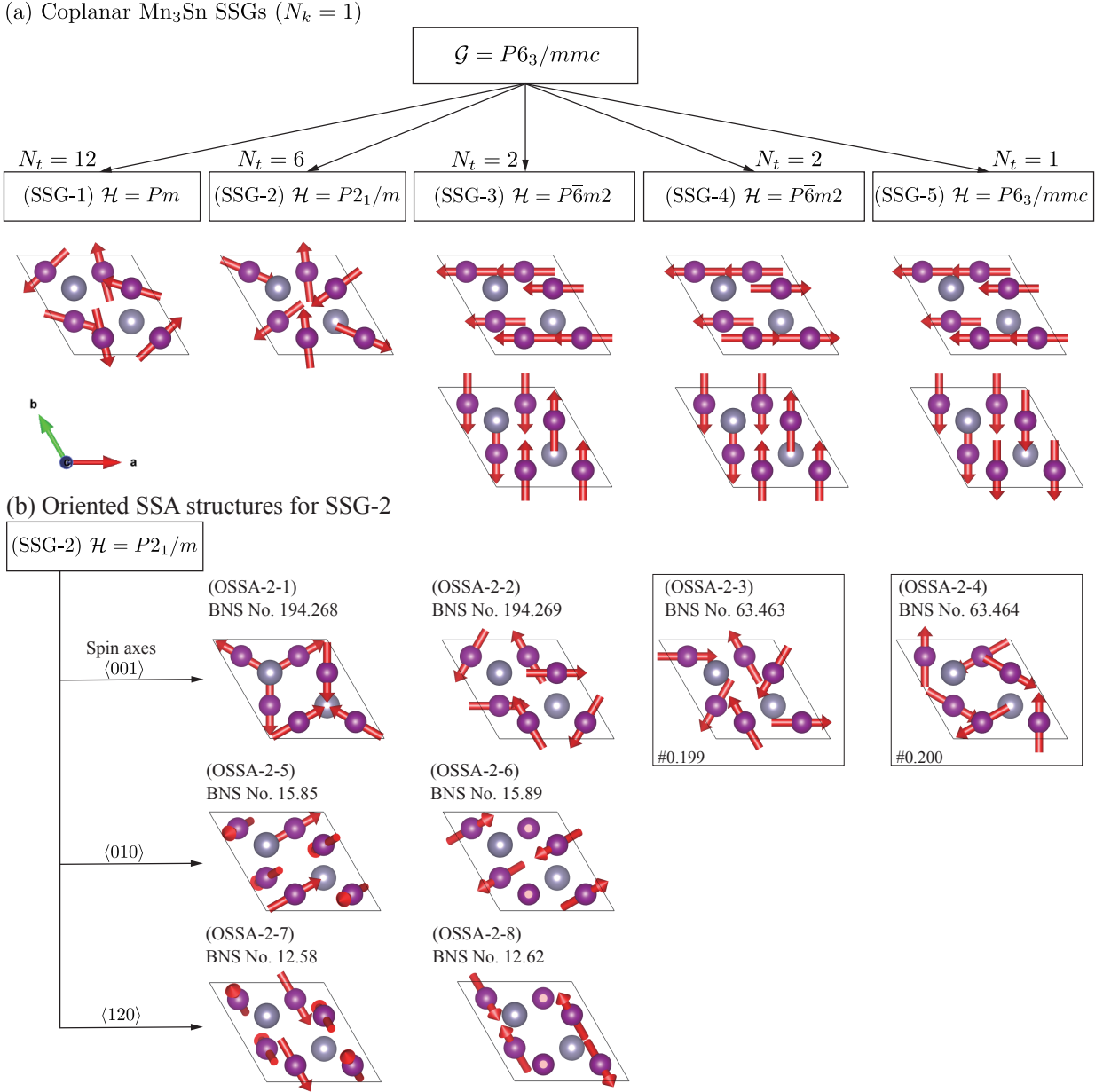


FIG. 2. Enumeration of coplanar magnetic structures of Mn_3Sn . (a) SSGs compatible with the nonmagnetic family space group $\mathcal{G} = P6_3/mmc$ (No. 194), coplanar, and $N_k = 1$. Five SSGs are obtained: SSG-1 with normal space subgroup $\mathcal{H} = Pm$ (No. 6), SSG-2 with $\mathcal{H} = P2_1/m$ (No. 11), SSG-3 and SSG-4 with $\mathcal{H} = P\bar{6}m2$ (No. 187), and SSG-5 with $\mathcal{H} = P6_3/mmc$ (No. 194). For each SSG, SSA structures from linearly independent symmetry-adapted magnetic moment bases are shown beneath the corresponding boxes. (b) Coplanar oriented SSA structures derived from SSG-2 and its enantiomeric one. For three inequivalent crystallographic orientations of the coplanar spin axis, eight oriented SSA structures (OSSA-2-1 to OSSA-2-8) are obtained in total. For $\langle 001 \rangle$, four oriented SSA structures appear, among which OSSA-2-3 (BNS No. 63.463) and OSSA-2-4 (BNS No. 63.464) correspond to the experimentally reported magnetic structures of Mn_3Sn in MAGNDATA entries #0.199 and #0.200, respectively. For $\langle 010 \rangle$ and $\langle 120 \rangle$, two oriented SSA structures are generated for each direction.

unit cell, their spin rotation parts are inequivalent. SSG-1 and SSG-2 yield one-dimensional symmetry-adapted magnetic moments, respectively. SSG-3 to SSG-6 yield two-dimensional symmetry-adapted magnetic moments.

We further derive oriented SSA structures from SSG-2 as illustrated in Fig. 3. This generates three inequivalent noncoplanar oriented SSA structures (OSSA-2-1 to OSSA-2-3), among which OSSA-2-2 corresponds to the

experimentally reported all-in-all-out magnetic structure of CoTa_3S_6 in entry #3.25 of MAGNDATA.

V. APPLICATION TO MAGNCDATA DATABASE

We apply the generation scheme to the MAGNDATA database, which contains experimentally reported magnetic structures. We first outline a classification scheme and present the resulting analysis. We then discuss materials that are not readily addressed within our framework.

A. Classification scheme

The MAGNCDATA database comprises 2,186 magnetic structures in total. Structures satisfying any of the following conditions fall outside the scope of the present study and are excluded from the analysis: (1) disordered structures containing sites with partial occupancy (2) non-AFM structures for which the ratio of the total magnetization to the absolute magnetization exceeds 1% (3) structures in which magnetic atoms occupy multiple inequivalent Wyckoff positions of the parent space group. We note that structures classified under condition (3) contain magnetic atoms that are not symmetry-related, and thus, these systems are beyond the applicability of any symmetry-based approach and are not considered further.

After applying these screening criteria, 1,023 structures remain, which are classified into the following five classes. Throughout this study, symmetry identification is performed using MOYOPY and SPINSPG packages [103, 122] with `symprec` = 1×10^{-4} and `mag_symprec` = 1×10^{-2} .

- `lower_family_translation_group`: structures in which the translation group of the family space group is smaller than that of the parent space group.
- `lower_family_point_group`: structures in which the point group of the family space group is smaller than that of the parent space group.
- `multiple_basis`: cases in which the totally symmetric representation of the SSG admits multiple linearly independent basis functions.
- `ssg_matched`: structures outside the above three classes, which are reproducible as SSA structures up to $O(3)$ transformations.
- `oriented_ssg_matched`: structures that belong to the `ssg_matched` class and are reproducible as oriented SSA structures.

Note that mcif files in MAGNCDATA contain either the crystal structure corresponding to the magnetically ordered phase or that of the disordered phase. In the former case, symmetry-identification procedures may fail

TABLE I. Classification of the 1,023 magnetic structures listed in MAGNDATA and considered in this study.

| | |
|---|-----|
| <code>lower_family_translation_group</code> | 66 |
| <code>lower_family_point_group</code> | 168 |
| <code>multiple_basis</code> | 166 |
| <code>ssg_matched</code> | 623 |
| <code>oriented_ssg_matched</code> | 511 |

to correctly determine the parent space group and the primitive cell owing to distortions induced by magnetic ordering, which in some cases affect the above symmetry classification. Although such cases could, in principle, be incorporated into the analysis by providing structural information for the disordered phase, we do not apply such a procedure in the present study for simplicity.

The benchmark analysis using spin density functional theory (SDFT) calculations in Sec. VI is carried out for materials belonging to `ssg_matched` and `oriented_ssg_matched`. Magnetic structures classified as `lower_family_translation_group`, `lower_family_point_group`, and `multiple_basis` are discussed in Sec. VC.

B. Summary of classification

The summary of the classification is presented in Table I, and the complete list is provided in Appendix E. Following the screening conditions described in Sec. VA, we find that, among the 2,186 magnetic structures listed in MAGNCDATA, 1,023 structures are suitable for the present analysis. Of these, 623 structures are classified as `ssg_matched`, which should be reproducible, at least up to $O(3)$, within the scheme described in Sec. II. Indeed, by explicitly performing the generation, we confirm that the corresponding structures reported in MAGNCDATA are successfully reproduced. Among these 623 `ssg_matched` structures, 511 belong to maximal MSGs of the corresponding SSGs and are classified as `oriented_ssg_matched`. This indicates that the SOC-induced locking of the spin axis is correctly reproduced for 82% of the materials, which constitutes one of the main results of this work.

As shown below, magnetic structures classified as `lower_family_point_group` are also reproducible by using all \mathcal{G}'_0 (see Sec. IID for its definition) as the target family space group, while maintaining a finite number of generation trials. Including these cases, the overall reproducibility at the SSG level reaches $(623 + 168)/1023 \simeq 77\%$, which supports the reliability of the present scheme. In contrast, the cases classified as `multiple_basis` require continuous tuning of internal parameters; consequently, it is fundamentally difficult to predict them within a symmetry-based framework using a finite number of trials. In addition, as discussed below, the structures classified as

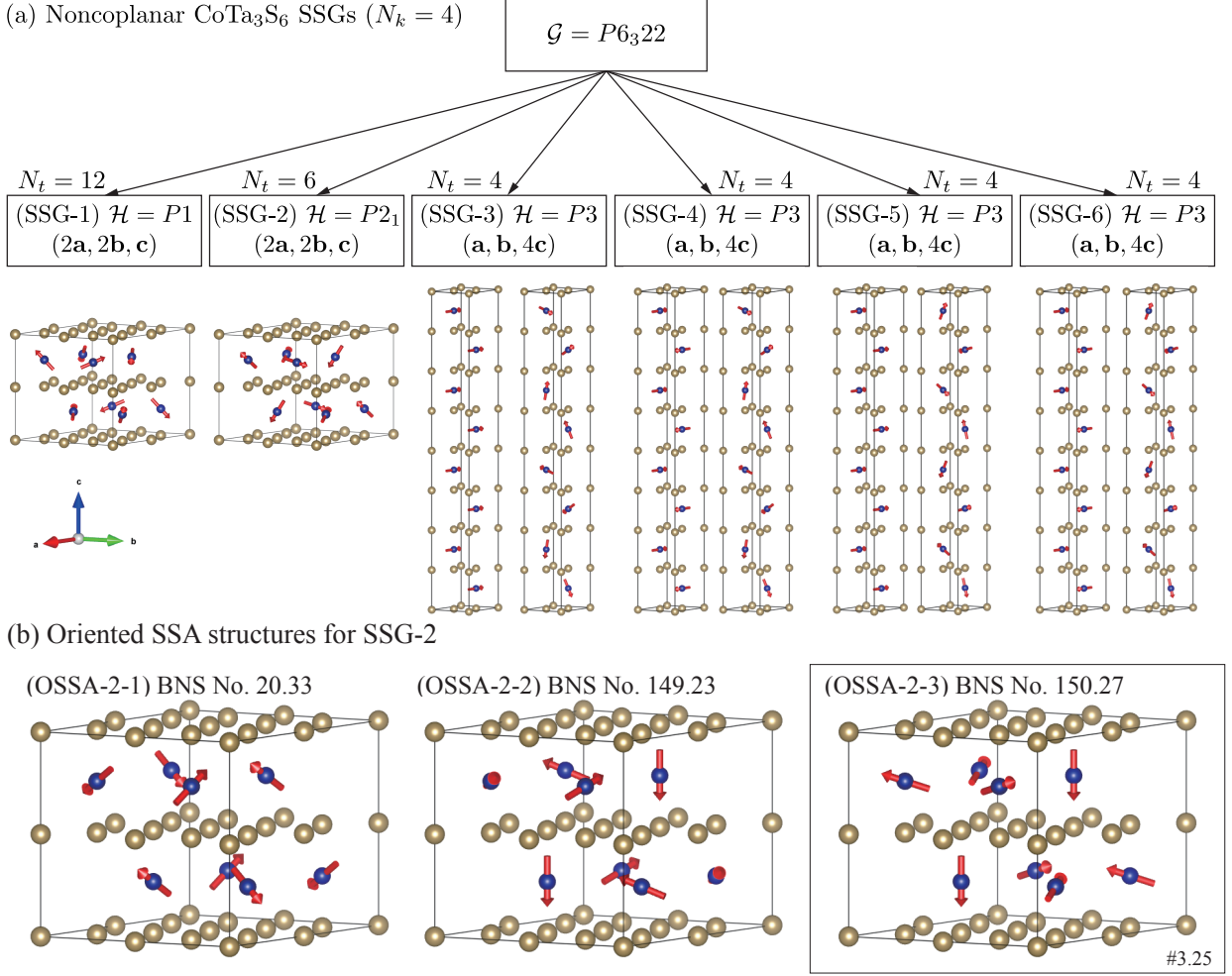


FIG. 3. Enumeration of noncoplanar magnetic structures of CoTa_3S_6 . (a) SSGs compatible with the nonmagnetic family space group $\mathcal{G} = P6_322$ (No. 182), noncoplanar, and $N_k = 4$. Six SSGs are obtained: SSG-1 with normal space subgroup $\mathcal{H} = P1$ (No. 1) and $2 \times 2 \times 1$ magnetic unit cell, SSG-2 with $\mathcal{H} = P2_1$ (No. 4) and $2 \times 2 \times 1$ magnetic unit cell, and SSG-3 to SSG-6 with $\mathcal{H} = P3$ (No. 143) and $1 \times 1 \times 4$ magnetic unit cell. For each SSG, SSA structures from linearly independent symmetry-adapted magnetic moment bases are shown beneath the corresponding boxes. (b) Noncoplanar oriented SSA structures generated from SSG-2. Three distinct oriented SSA structures (OSSA-2-1 to OSSA-2-3) are obtained, among which OSSA-2-2 (BNS No. 150.27) corresponds to the experimentally reported magnetic structure of CoTa_3S_6 in MAGNDATA entry #3.25. The nonmagnetic atoms of sulfur are not shown for clarity.

`lower_family_translation_group` cannot be addressed by the present method. Together, these cases account for 234 out of the 1,023 structures.

C. Examples not classified as `ssg_matched`

Here, we present representative examples of magnetic structures that are not classified as `ssg_matched`.

1. DyB_4

Figure 4(a) shows the magnetic structure of DyB_4 in MAGNDATA entry #0.22, and Figs. 4(b)-(d) show the SSA structures with $N_k = 1$. The parent point group of DyB_4 is $4/mmm$, and the SSA structures share the same family point group. Consistent with this symmetry, the structures shown in Figs. 4(b), (c) and (d) are invariant under, for example, $((4^+_{001}, \mathbf{0}), 1), ((4^+_{001}, \mathbf{0}), \bar{1})$ and $((4^+_{001}, \mathbf{0}), 4^-_{001})$, respectively. In contrast, the experimental structure shown in Fig. 4(a) lacks the spatial four-fold symmetry and therefore falls into the `lower_family_point_group` class. However, the point

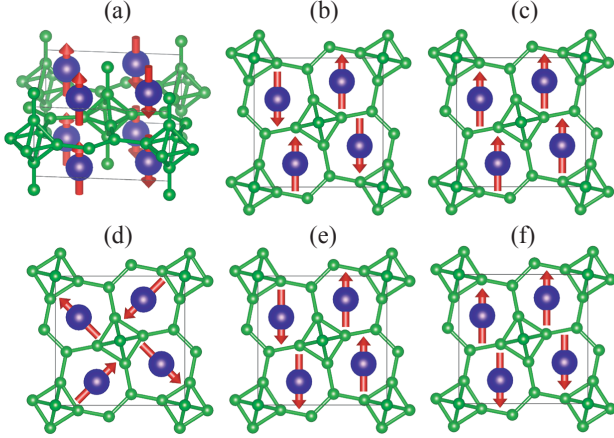


FIG. 4. Magnetic structures of DyB₄. (a) Magnetic structures of DyB₄ reported in MAGNDATA entry #0.22. (b)-(d) Three SSA structures with $N_k = 1$, whose family space group $G = P4/mbm$ (No. 127) is identical to the space group. (e) and (f) Two SSA structures with the family space group $G = Pbam$ (No. 55).

group mmm is a subgroup of $4/mmm$ that does not induce Wyckoff-position splitting at the Dy site and is the family point group of Fig. 4(a). Accordingly, this structure can be reproduced while keeping the fixed moment-size condition. Figures 4(e) and (f) show magnetic structures obtained by using a maximal t-subgroup $G'_0 = Pbam$ as the target family space group, with Fig. 4(f) being identical to Fig. 4(a). As illustrated by this example, magnetic structures belonging to the `lower_family_point_group` class are tractable within the present approach. In the case of DyB₄, relaxing the condition on the target family space group increases the number of SSA structures only from three to five.

For cases with $N_k > 1$, there exist combinations of a space group and Wyckoff positions for which no SSA structure has a family space group identical to the parent space group. Following the treatment described in Sec. II D, we then search for maximal t-subgroups and attempt magnetic structure generation. We find that 27 out of 166 cases are successfully reproduced using this procedure.

2. CoSO₄

Figure 5(a) shows the magnetic structure of CoSO₄ reported in MAGNDATA entry #0.96, and Figs. 5(b)-(e) show the SSA structures with $N_k = 1$. It is readily seen that the magnetic structure shown in Fig. 5(a) can be expressed as a linear combination of those in Figs. 5(c)-(e) and therefore belongs to the `multiple_basis` class. In such cases, the coefficients in the linear combination are continuous parameters, and consequently an identical magnetic structure cannot be generated by any symmetry-based construction. Nevertheless, in situ-

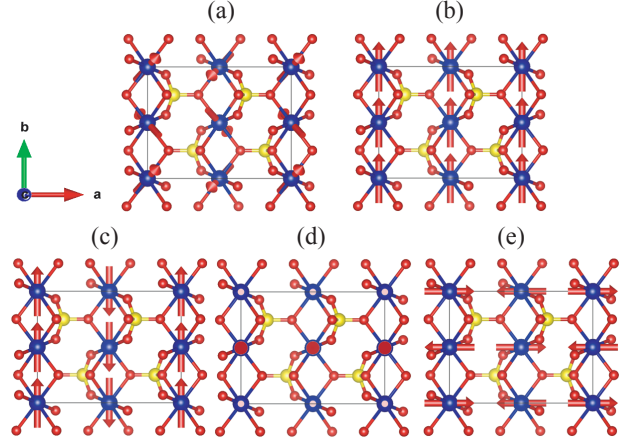


FIG. 5. Magnetic structures of CoSO₄. (a) Magnetic structures of CoSO₄ reported in MAGNDATA entry #0.96. (b)-(e) Four SSA structures with $N_k = 1$, whose family space group $G = Pnma$ (No. 62) is identical to the space group. (c)-(e) correspond to collinear AFMs characterized by modulation directions [100], [010], and [110], respectively.

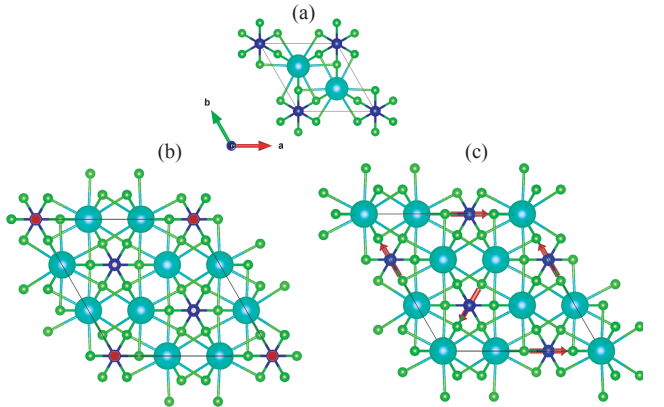


FIG. 6. Magnetic structure of CsCoCl₃. (a) Primitive unit cell of CsCoCl₃. (b) Magnetic structure of CsCoCl₃ reported in MAGNDATA entry #1.0.9, whose family space group is $G = P63/mcm$ (No. 193). (c) An SSA structure with $N_k = 3$ and family space group $G = P63/mmc$ (No. 194), which is identical to the space group.

tions where one magnetic configuration is dominant and the others are only weakly induced as in canted AFMs, the correct magnetic structure may still emerge during self-consistent calculations. We therefore emphasize that not all `multiple_basis` cases are entirely intractable within the present framework.

3. CsCoCl₃

Here, we consider the case of CsCoCl₃ (Fig. 6). The primitive unit cell is shown in Fig. 6(a), and the magnetic structure in MAGNDATA entry #1.0.9 is shown in Fig. 6(b). Figure 6(c) presents one of the SSA struc-

tures with $N_k = 3$. Both structures shown in Figs. 6(b) and (c) have a magnetic unit cell that is three times larger than the primitive cell. However, while the SSA structure preserves the family space group $\mathcal{G} = P6_3/mmc$ (No. 194), which is identical to the space group of the nonmagnetic structure, the experimental magnetic structure has a different family space group $\mathcal{G} = P6_3/mcm$ (No. 193). The SSA structure is characterized by a helical spin texture associated with a spin translation vector $\mathbf{k} = (1/3, 1/3, 0)$, whereas the experimental structure is not because the up–up–down collinear spin alignment cannot be represented by any spin translation. Consequently, the family translation group of CsCoCl_3 is reduced by a factor of three, and the structure is assigned to the `lower_family_translation_group` class.

Within the framework described in Sec. II, we consider the space group or its maximal t-subgroups as the family space group of the SSA structures, and thus, cell expansions not associated with spin translations cannot be treated. Therefore, the magnetic structures in the `lower_family_translation_group` class are not reproducible by the present approach. We finally note that some cases assigned to this class originate from ambiguities in identifying the primitive cell, as discussed at the end of Sec. V A; therefore, not all 66 cases in this class are necessarily beyond the reach of the present approach.

VI. HIGH-THROUGHPUT CALCULATIONS

In this section, we present benchmarks for the first-principles magnetic structure prediction method using the proposed scheme. For materials classified as `ssg_matched`, we generate SSA and oriented SSA structures and then perform high-throughput SDFT calculations. Based on the results, we discuss the computational efficiency and the predictive performance of the proposed scheme.

A. Details of the computation

We used the ATOMATE2 package [123, 124] to manage the calculations, which internally utilizes the PYMATGEN, CUSTODIAN, and FIREWORKS libraries [125, 126]. Electronic structure calculations were carried out using the Vienna *ab initio* Simulation Package (VASP) [127]. Throughout this study, we employed the Perdew-Burke-Ernzerhof exchange-correlation functional [128] with projector augmented-wave pseudopotentials [129, 130], without applying a Hubbard- U correction.

In practice, self-consistent field (SCF) calculations without SOC were first performed for the SSA structures. Subsequently, SOC was included, and non-SCF calculations were carried out for the descendant oriented SSA structures, employing fixed charge densities obtained from the preceding SCF calculations. We note that oriented SSA structures can be obtained by global

TABLE II. Summary of computational performance of SDFT calculations. SSG and Oriented SSG correspond to SCF without SOC and non-SCF with SOC calculations, respectively.

| | SSG | Oriented SSG |
|---------------------------------|-----|--------------|
| Number of calculations | 876 | 2370 |
| Unconverged calculations | 1 | 0 |
| Magnetic-structure change > 10% | 57 | 189 |

$SO(3)$ spin rotations applied to the corresponding SSA structures, for which VASP provides an SCF-to-non-SCF workflow via the `SAXIS` flag. However, because `SAXIS` merely defines the spin-quantization axis and does not allow arbitrary $SO(3)$ rotations, we modified the code to accept the Euler angles as input and to apply the corresponding rotations to the magnetic moments prior to the non-SCF calculations. This extension significantly improved both the computational efficiency and the stability of the oriented SSG-based calculations.

The remaining VASP input parameters for the SCF calculations were set as follows: `ENCUT` = 1.2 times the maximum `ENMAX` value in the `POTCAR` file, `ALGO` = `ALL`, `ISEARCH` = 0, `ISMEAR` = 0, `SIGMA` = 0.02, `LASPH` = `True`, `LMIXTAU` = `True`, `LMAXMIX` = 6, `PREC` = `Accurate`, `LNONCOLLINEAR` = `True`, `NELM` = 200, `KPAR` = 6, `NPAR` = 2, and `EDIFF` = 2×10^{-5} . For the subsequent non-SCF calculations, only the following parameters were modified: `ALGO` = `Normal`, `EDIFF` = 1×10^{-7} , `ICHARG` = 11, `LSORBIT` = `True`. The pseudopotentials were chosen according to the default recommendations of `PBE_64`, while open-core pseudopotentials were used for $4f$ and $5f$ elements. Brillouin-zone integrations were performed using a Γ -centered \mathbf{k} -point grid generated by PYMATGEN, with a reciprocal density of 120 \AA^{-3} . The number of MPI processes was fixed to 24 for all calculations. For unconverged cases, additional calculations were performed with input modifications guided by the default error-handling settings implemented in the CUSTODIAN code.

B. Summary of the calculations

From the 623 structures classified as `ssg_matched`, we further selected a subset of materials according to the following criteria: (1) the number of atoms in the magnetic unit cell is fewer than 30; (2) $4f$ and $5f$ elements are not magnetic; and (3) in cases where multiple entries share the same crystal structure, only one representative is retained. Applying these criteria, we obtained a total of 283 distinct materials; the full list is provided in Appendix E. Among them, 226 materials additionally satisfy the `oriented_ssg_matched` condition. For the 283 `ssg_matched` materials, we generated 876 SSA structures and 2370 descendant oriented SSA structures. As a result, 876 SCF calculations without SOC and 2370 non-SCF calculations with SOC were performed in this study. For simplicity, the structure generation was restricted to magnetic structures with the same k -index

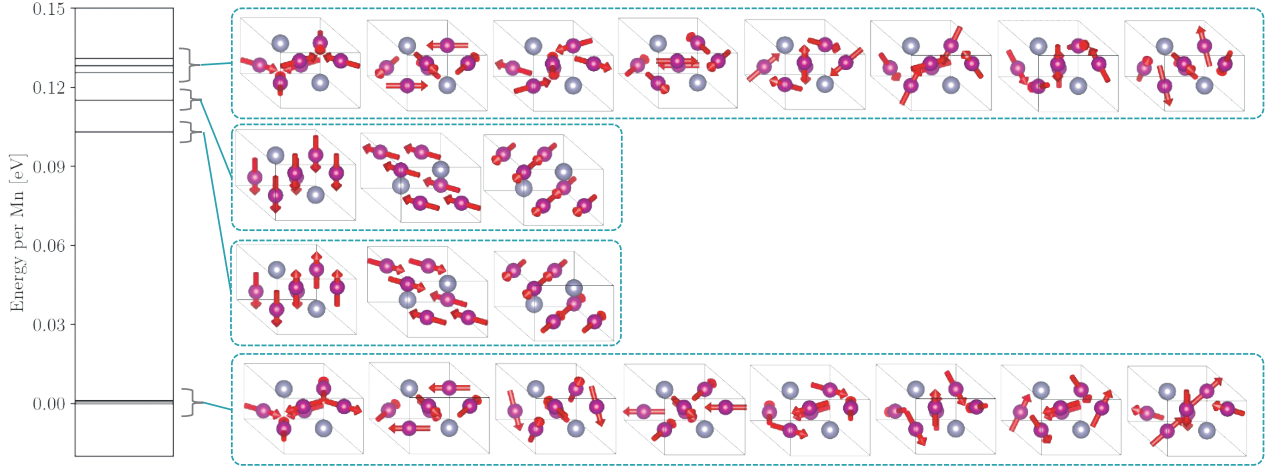


FIG. 7. Oriented SSA structures with $N_k = 1$ and their energy levels of Mn_3Sn . The structures enclosed by dashed lines are generated from the same SSG, in particular, the lowest-energy manifold corresponds to the SSG-2 structure shown in Fig. 2.

N_k as reported in MAGNDATA.

Table II summarizes the computational performance of SDFT calculations. Under the conditions described in Sec. VIA, only one calculation failed to converge (entry #1.461). In contrast, all non-SCF calculations converged successfully. Even among the converged cases, the magnetic structure sometimes changes during the calculation. In the present case, the converged magnetic structure deviates by more than 10% from the input structures in 57 out of 876 SCF calculations and in 189 out of 2370 non-SCF calculations. We note that the latter includes cases in which the magnetic structure had already changed during the SCF stage, and therefore the fraction of changes attributable solely to the non-SCF calculations is much smaller.

Regarding the computational cost, the 876 SCF calculations required a total of approximately 650 hours (wall-clock time) on 24 cores, whereas the non-SCF calculations consumed about 400 hours. Considering that the number of non-SCF calculations is roughly three times larger than that of SCF and that the convergence criteria (EDIFF in the input) are 200 times tighter, this result clearly demonstrates the high efficiency of the fixed-charge approach adopted in this study. We also note that, without fixing the charge density, electronic-structure calculations with SOC may relax into local minima that differ from those obtained in the calculations without SOC. From this perspective, even though it can lead to an underestimation of SOC effects, the fixed-charge approach is essential for achieving stable total-energy evaluations, as recommended for magnetic anisotropy calculations in the VASP documentation.

TABLE III. Summary of the predictive performance of SDFT calculations. Typical energy differences of the manifold are given in units of meV per magnetic atom. $\bar{\Delta}$ is the average energy difference estimated from the standard deviation.

| | SSG | Oriented SSG |
|--------------------------------|-----|--------------|
| Number of materials | 283 | 226 |
| Correctly identified materials | 232 | 172 |
| $\bar{\Delta}$ | 103 | 0.29 |

C. Predictive performance

Here, we present results for the predictive performance of the SDFT calculations. Related analyses based on the cluster multipole method were previously reported by some of the present authors [69], and more recently, RA-based analyses were reported in Ref. [131]; both studies focused exclusively on structures with $N_k = 1$. In contrast, the calculations performed here include 175 cases with $N_k = 1$ and 108 cases with $N_k > 1$.

The results are summarized in Table III. Among the 283 materials classified as `ssg_matched`, 232 materials ($\sim 82\%$) were correctly identified as having one of their experimentally observed magnetic structures as energetically most stable. Among the 226 materials classified as `oriented_ssg_matched`, 172 materials ($\sim 76\%$) were found to have oriented SSA structures identical to the reported one, lying within the set of energetically most stable configurations. We note that energy comparisons among oriented SSA structures require resolving small energy differences induced by SOC. Given the intrinsic accuracy of SDFT, it is necessary to introduce an appropriate energy tolerance to judge the agreement with the reported structures. In the present analysis, we adopt a threshold of $30 \mu\text{eV}$ per magnetic atom, chosen as one tenth of the typical SOC energy scale (see the following discussion). From these results, the reliability of SDFT

for assessing the stability of magnetic structures is on the order of 80%, both in terms of SSG and oriented SSG descriptions. It should be noted, however, that this figure is not absolute, as it may vary depending on the choice of the Coulomb $+U$ correction and the exchange-correlation functional.

Next, we discuss the energy differences among SSA structures and those among oriented SSA structures, which are required to validate the two-step prediction: SCF calculations without SOC are first used to identify the most stable SSA structure, followed by non-SCF calculations with SOC to resolve the oriented SSA structure manifold. As discussed above, energy differences among oriented SSA structures are expected to scale with SOC and are therefore much smaller than those among SSA structures. As an example, Fig. 7 shows the magnetic structures of Mn_3Sn together with the corresponding energy differences. As can be seen, Mn_3Sn exhibits a clear separation of energy scales: the inclusion of SOC does not lead to a reordering of the energy levels among different SSA structures. More systematic results are shown in Table III. Here, we focus only on cases where the converged magnetic structures agree with the initial ones. The average energy difference $\bar{\Delta}$ among SSA structures, estimated from the standard deviation, is approximately 103 meV per magnetic atom. In contrast, $\bar{\Delta}$ among oriented SSA structures is about 290 μeV per magnetic atom, indicating a separation of energy scales by nearly a factor of 300. In fact, among the 226 materials classified as `oriented_ssg_matched`, only two cases (entries #0.916 and #1.382) were found in which the energetically most stable SSA structure was altered by the inclusion of SOC. This clear hierarchy demonstrates that, at least for the d -electron magnetic materials considered in this study, the proposed scheme is well justified.

VII. CONCLUSION

We have presented a framework for the systematic generation of magnetic structures inspired by the concept of oriented SSGs. A key advantage of the SSG-based formulation is that it can naturally enforce the fixed-moment condition on symmetry-equivalent sites, thereby enabling an exhaustive enumeration of magnetically inequivalent structures up to global $O(3)$ transformations. Building on the oriented SSG concept, we further introduced a practical procedure for constructing magnetic structures that are inequivalent under the parent space group and are thus suitable for resolving SOC-induced energy splittings.

Applying the method to the MAGNDATA database, we classified 1,023 reported magnetic structures into five categories and showed typical examples for which our scheme has limited applicability. For a computationally tractable set of 283 materials, we performed SDFT calculations using a two-step workflow [102]: SCF calculations without SOC for the SSA structures, followed by fixed-

charge non-SCF calculations with SOC for the descendant oriented SSA structures obtained through global $SO(3)$ rotations of the parent SSA structures. This workflow provides high numerical stability and favorable computational efficiency, as summarized in Sec. VI B.

The benchmark results quantify the practical reliability of first-principles magnetic-structure prediction in a broad dataset. At the SSG level, the experimentally reported structures are identified as energetically stable in 82% of the examined materials. At the oriented SSG level, the corresponding success rate is 76%. Importantly, we found a clear separation of energy scales: typical energy differences among distinct SSA structures are around 100 meV per magnetic atom, whereas those among oriented SSA structures are around 0.3 meV per magnetic atom, indicating an SOC-induced hierarchy by roughly a factor of 300. Consistent with this hierarchy, only a very small fraction of materials exhibit a reordering of the lowest-energy SSA structure upon inclusion of SOC.

These findings establish oriented SSG-based enumeration, combined with first-principles calculations within a two-step strategy, as a robust and efficient framework for large-scale magnetic-structure prediction. The proposed approach is applicable to systematic searches for AFMs with targeted symmetry properties and provides a quantitative baseline for assessing the accuracy limits of SDFT-based magnetic-structure predictions. Future extensions to magnetic structures classified in `lower_family_translation_group` and `multiple_basis` classes, as well as the inclusion of correlation effects (e.g., $+U$) in SDFT, will further broaden the applicability and strengthen symmetry-guided high-throughput approaches.

An implementation of the present algorithm is distributed under a permissive free software license in SPINFORGE, available at <https://github.com/spglib/spinforge>¹.

VIII. ACKNOWLEDGMENTS

Figures of magnetic structures are created using VESTA [132]. This work is supported by JSPS-KAKENHI (No. JP21H04990, JP23K13058, JP24K00581, JP25K21684, JP25H00420, JP25H01246, JP25H01252, JP25H02115), JST-ERATO (No. JPMJER2503), JST-MIRAI (No. JPMJMI20A1), JST-CREST (No. JPMJCR23O4), JST-ASPIRE (No. JPMJAP2317), and the RIKEN TRIP initiative (RIKEN Quantum, Advanced General Intelligence for Science Program, Many-body Electron Systems). The authors acknowledge the use of the AI-based writing tool ChatGPT (OpenAI, version 5.2) for language polishing. The

¹ We plan to release it after the publication of this paper.

authors take full responsibility for the content of this manuscript.

Appendix A: Detailed algorithm for enumerating spin space groups

We continue the discussion in Sec. II B to enumerate SSGs from a given family space group \mathcal{G} , a spin-only group \mathcal{B}_{so} , and a k-index N_k . Although the following algorithm is essentially the same as that in Refs. [80–82], we here provide a self-contained and more implementation-friendly description usable for on-the-fly SSG enumeration. This simplification partly arises from restricting equivalence to conjugacy under $\mathcal{G} \times O(3)$, rather than group isomorphism under $\mathcal{N}(\mathcal{G}) \times O(3)$.

The overall procedure to enumerate SSGs is as follows. We introduce notation for space group \mathcal{G} in Sec. A 1. We enumerate normal t-subgroups \mathcal{M} of \mathcal{G} in Sec. A 2. We enumerate normal k-subgroups \mathcal{H} of \mathcal{M} with $\mathcal{H} \trianglelefteq \mathcal{G}$ in Sec. A 3. Finally, we enumerate injective homomorphisms $U : \mathcal{G}/\mathcal{H} \rightarrow O(3)/\mathcal{B}_{\text{so}}$ by reducing the problem to enumeration of faithful orthogonal representations of \mathcal{G}/\mathcal{H} in Sec. A 4.

1. Group structure of family space group

We prepare notation for the family space group \mathcal{G} . We write the point group of \mathcal{G} as

$$\mathcal{P}(\mathcal{G}) = \{\mathbf{R}_i \mid (\mathbf{R}_i, \boldsymbol{\tau}_i)\mathcal{T}(\mathcal{G}) \in \mathcal{G}/\mathcal{T}(\mathcal{G})\}. \quad (\text{A1})$$

We denote a lattice formed by translation subgroup $\mathcal{T}(\mathcal{G})$ as

$$\mathcal{L}_{\mathcal{G}} = \{\mathbf{t} \mid (\mathbf{I}, \mathbf{t}) \in \mathcal{T}(\mathcal{G})\}. \quad (\text{A2})$$

Let $\boldsymbol{\tau}_{\bullet} : \mathcal{P}(\mathcal{G}) \rightarrow \mathbb{R}^3$ be a translation part of \mathcal{G} with $\boldsymbol{\tau}_{\mathbf{R}_i} = \boldsymbol{\tau}_i$. For coset representatives g_i and g_j , we choose an index $ij \in \{1, \dots, n\}$ such that $\mathbf{R}_{ij} = \mathbf{R}_i \mathbf{R}_j \in \mathcal{P}(\mathcal{G})$. Then, we define a factor system for a group extension of $\mathcal{P}(\mathcal{G})$ by $\mathcal{T}(\mathcal{G})$ as

$$g_i g_j = (\mathbf{I}, \boldsymbol{\sigma}(i, j)) g_{ij} \quad (\text{A3})$$

with

$$\boldsymbol{\sigma}(i, j) = \boldsymbol{\tau}_i + \mathbf{R}_i \boldsymbol{\tau}_j - \boldsymbol{\tau}_{ij}. \quad (\text{A4})$$

2. Normal t-subgroup of \mathcal{G}

We enumerate normal subgroups \mathcal{P}' of $\mathcal{P}(\mathcal{G})$ by brute-force search with memoization. Since the number of subgroups of an order- n group is bounded by $\exp(O((\log n)^2))$ [133] and $|\mathcal{P}(\mathcal{G})| \leq 48$ for three-dimensional crystallographic point groups, this step is computationally tractable.

For each normal subgroup \mathcal{P}' , we denote the coset decomposition of $\mathcal{P}(\mathcal{G})$ by \mathcal{P}' as

$$\mathcal{P}(\mathcal{G}) = \bigcup_{I=1}^{N_t} \mathbf{R}_{i_I} \mathcal{P}', \quad (\text{A5})$$

where $N_t = |\mathcal{P}(\mathcal{G}) : \mathcal{P}'|$ and $\{\mathbf{R}_{i_I}\}_{I=1}^{N_t}$ are representatives of the cosets. Then, we construct a t-subgroup \mathcal{M} of \mathcal{G} as

$$\mathcal{M} = \bigcup_{\mathbf{R}_h \in \mathcal{P}'} g_h \mathcal{T}(\mathcal{G}). \quad (\text{A6})$$

While \mathcal{M} is a t-subgroup of \mathcal{G} by construction, we need to check whether \mathcal{M} is normal in \mathcal{G} . That is, for all pairs of $g_{i_I} \mathcal{M} \in \mathcal{G}/\mathcal{M}$ and $g_h \mathcal{T}(\mathcal{G}) \in \mathcal{M}/\mathcal{T}(\mathcal{G})$, we require $g_{i_I}^{-1} g_h g_{i_I} \in \mathcal{M}$. This condition is equivalent to requiring that

$$\boldsymbol{\tau}_h + \mathbf{R}_h \boldsymbol{\tau}_{i_I} - \boldsymbol{\tau}_{i_I} = \mathbf{R}_{i_I} \boldsymbol{\tau}_{\mathbf{R}_{i_I}^{-1} \mathbf{R}_h \mathbf{R}_{i_I}} \pmod{\mathcal{L}_{\mathcal{G}}}, \quad (\text{A7})$$

where we use $\mathbf{R}_{i_I}^{-1} \mathbf{R}_h \mathbf{R}_{i_I} \in \mathcal{P}'$ because \mathcal{P}' is normal in $\mathcal{P}(\mathcal{G})$. In the following, we denote \mathcal{P}' satisfying Eq. (A7) as $\mathcal{P}_{\mathcal{M}}$.

Note that, for coset representatives \mathbf{R}_{i_I} and \mathbf{R}_{i_J} , their multiplication may not be a coset representative of $\mathcal{P}(\mathcal{G})/\mathcal{P}(\mathcal{M})$. We denote the index $h_{IJ} \in \{1, \dots, n\}$ such that

$$\mathbf{R}_{i_I i_J} = \mathbf{R}_{i_I} \mathbf{R}_{i_J} \mathbf{R}_{h_{IJ}}. \quad (\text{A8})$$

3. Normal space subgroup of \mathcal{G}

We enumerate normal sublattices \mathcal{L}' of $\mathcal{L}_{\mathcal{G}}$ under $\mathcal{P}(\mathcal{G})$ with a given k -index $N_k = |\mathcal{L}_{\mathcal{G}}/\mathcal{L}'|$. Inequivalent sublattices of $\mathcal{L}_{\mathcal{G}}$ are enumerated by Hermite normal forms of 3×3 integer matrices with determinant N_k [134]. The normality condition is expressed as

$$\mathbf{R}_i \mathcal{L}' = \mathcal{L}' \quad (\forall \mathbf{R}_i \in \mathcal{P}(\mathcal{G})), \quad (\text{A9})$$

and it can be checked by verifying that the basis vectors of $\mathbf{R}\mathcal{L}'$ and \mathcal{L}' are related by a unimodular matrix. We denote the translation subgroup formed by \mathcal{L}' as \mathcal{T}' , and coset representatives of $\mathcal{T}(\mathcal{G})/\mathcal{T}'$ as

$$\mathcal{T}(\mathcal{G}) = \bigcup_{m=1}^{N_k} (\mathbf{I}, \mathbf{t}_m) \mathcal{T}'. \quad (\text{A10})$$

Next, we consider a normal k-subgroup \mathcal{H} of \mathcal{M} with translation subgroups \mathcal{T}' . Although point groups of \mathcal{H} and \mathcal{M} are the same, their translation parts may differ up to $\mathcal{L}_{\mathcal{G}}$ [135]. Thus, we enumerate possible additional translation parts \mathbf{t}_{m_h} ($m_h \in \{1, \dots, N_k\}$) for each coset representative such that

$$\mathcal{H} = \bigcup_{\mathbf{R}_h \in \mathcal{P}(\mathcal{M})} \tilde{g}_h \mathcal{T}' \quad (\text{A11})$$

where $\tilde{g}_h = (\mathbf{R}_h, \tau_h + \mathbf{t}_{m_h})$. We denote the translation part of \tilde{g}_h as

$$\tilde{\tau}_h = \tau_h + \mathbf{t}_{m_h}. \quad (\text{A12})$$

For each pair of \tilde{g}_{h_1} and \tilde{g}_{h_2} , their multiplication

$$\begin{aligned} & \tilde{g}_{h_1} \tilde{g}_{h_2} \\ &= (\mathbf{I}, \tilde{\tau}_{h_1}) g_{h_1} (\mathbf{I}, \tilde{\tau}_{h_2}) g_{h_2} \\ &= (\mathbf{I}, \tilde{\tau}_{h_1} + \mathbf{R}_{h_1} \tilde{\tau}_{h_2}) g_{h_1} g_{h_2} \\ &= (\mathbf{I}, \tilde{\tau}_{h_1} + \mathbf{R}_{h_1} \tilde{\tau}_{h_2} + \boldsymbol{\sigma}(h_1, h_2)) g_{h_1} g_{h_2} \quad (\because \text{Eq. (A3)}) \end{aligned}$$

implies

$$\tilde{\tau}_{(h_1, h_2)} = \tilde{\tau}_{h_1} + \mathbf{R}_{h_1} \tilde{\tau}_{h_2} + \boldsymbol{\sigma}(h_1, h_2) \quad \text{mod } \mathcal{L}'. \quad (\text{A13})$$

Thus, we obtain a group \mathcal{H} by exhaustively assigning \mathbf{t}_m for each generator of $\mathcal{P}(\mathcal{M})$ and checking the condition of Eq. (A13) for all pairs of elements in $\mathcal{P}(\mathcal{M})$.

At this moment, \mathcal{H} may not be a group because associativity is not yet checked. Before checking the associativity condition, we first check the normality conditions of \mathcal{H} in \mathcal{M} and \mathcal{G} . If \mathcal{H} is normal in \mathcal{M} , then for all pairs of $\mathbf{R}_h \in \mathcal{P}(\mathcal{M})$ and $m \in \{1, \dots, N_k\}$, we require

$(\mathbf{I}, \mathbf{t}_m)^{-1} \tilde{g}_h (\mathbf{I}, \mathbf{t}_m) \in \mathcal{H}$. The multiplication leads to

$$\begin{aligned} (\mathbf{I}, \mathbf{t}_m)^{-1} \tilde{g}_h (\mathbf{I}, \mathbf{t}_m) &= (\mathbf{R}_h, \tilde{\tau}_h + \mathbf{R}_h \mathbf{t}_m - \mathbf{t}_m) \\ &= (\mathbf{I}, \mathbf{R}_h \mathbf{t}_m - \mathbf{t}_m) \tilde{g}_h. \end{aligned}$$

Thus, the normality condition of \mathcal{H} in \mathcal{M} is expressed as

$$\mathbf{R}_h \mathbf{t}_m = \mathbf{t}_m \quad \text{mod } \mathcal{L}_\mathcal{H}. \quad (\text{A14})$$

Similarly, if \mathcal{H} is normal in \mathcal{G} , then for all pairs of $g_{i_I} \mathcal{M} \in \mathcal{G}/\mathcal{M}$ and $\tilde{g}_h \mathcal{T}_\mathcal{H} \in \mathcal{H}/\mathcal{T}_\mathcal{H}$, we require $(\mathbf{I}, \mathbf{t}_m)^{-1} g_{i_I}^{-1} \tilde{g}_h g_{i_I} (\mathbf{I}, \mathbf{t}_m) \in \mathcal{H}$. The multiplication leads to

$$\begin{aligned} & (\mathbf{I}, \mathbf{t}_m)^{-1} g_{i_I}^{-1} \tilde{g}_h g_{i_I} (\mathbf{I}, \mathbf{t}_m) \\ &= g_{i_I}^{-1} (\mathbf{I}, \mathbf{R}_{i_I} \mathbf{t}_m)^{-1} \tilde{g}_h (\mathbf{I}, \mathbf{R}_{i_I} \mathbf{t}_m) g_{i_I} \\ &= g_{i_I}^{-1} \tilde{g}_h g_{i_I} \quad \text{mod } \mathcal{L}_\mathcal{H} \quad (\because \text{Eq. (A14)}) \\ &= (\mathbf{R}_{i_I}^{-1} \mathbf{R}_h \mathbf{R}_{i_I}, \mathbf{R}_{i_I}^{-1} (\tilde{\tau}_h + \mathbf{R}_h \tau_{i_I} - \tau_{i_I})) \quad \text{mod } \mathcal{L}_\mathcal{H}. \end{aligned}$$

Thus, the normality condition of \mathcal{H} in \mathcal{G} is expressed as

$$\tilde{\tau}_h + \mathbf{R}_h \tau_{i_I} - \tau_{i_I} = \mathbf{R}_{i_I} \tilde{\tau}_{\mathbf{R}_{i_I}^{-1} \mathbf{R}_h \mathbf{R}_{i_I}} \quad \text{mod } \mathcal{L}_\mathcal{H}, \quad (\text{A15})$$

where we define $\tilde{\tau}_\bullet : \mathcal{P}(\mathcal{M}) \rightarrow \mathbb{R}^3$ as the translation part of \mathcal{H} with $\tilde{\tau}_{\mathbf{R}_h} = \tilde{\tau}_h$.

We consider a group multiplication of cosets of \mathcal{M}/\mathcal{H} by

$$\begin{aligned} g_{i_I} g_{i_J} \mathcal{H} &= (\mathbf{I}, \boldsymbol{\sigma}(i_I, i_J)) g_{i_I i_J} \mathcal{H} \quad (\because \text{Eq. (A3)}) \\ &= (\mathbf{I}, \boldsymbol{\sigma}(i_I, i_J)) g_{i_I i_J} g_{h_{IJ}} g_{h_{IJ}}^{-1} \mathcal{H} \quad (\because \text{Eq. (A8)}) \\ &= (\mathbf{I}, \boldsymbol{\sigma}(i_I, i_J) + \boldsymbol{\sigma}(i_I i_J, h_{IJ})) g_{i_I i_J} g_{h_{IJ}}^{-1} \mathcal{H} \\ &= (\mathbf{I}, \boldsymbol{\sigma}(i_I, i_J) + \boldsymbol{\sigma}(i_I i_J, h_{IJ})) g_{i_I i_J} ((\mathbf{I}, -\mathbf{t}_{m_{h_{IJ}}}) \tilde{g}_{h_{IJ}})^{-1} \mathcal{H} \\ &= (\mathbf{I}, \boldsymbol{\sigma}(i_I, i_J) + \boldsymbol{\sigma}(i_I i_J, h_{IJ}) + \mathbf{R}_{i_I i_J} \mathbf{t}_{m_{h_{IJ}}}) g_{i_I i_J} \mathcal{H} \quad (\because \text{Eq. (A14)}). \end{aligned}$$

Thus, the group multiplication of \mathcal{M}/\mathcal{H} is expressed as

$$g_{i_I} g_{i_J} \mathcal{H} = (\mathbf{I}, \mathbf{s}(i_I, i_J)) g_{i_I i_J} \mathcal{H} \quad (\text{A16})$$

with

$$\mathbf{s}(i_I, i_J) = \boldsymbol{\sigma}(i_I, i_J) + \boldsymbol{\sigma}(i_I i_J, h_{IJ}) + \mathbf{R}_{i_I i_J} \mathbf{t}_{m_{h_{IJ}}}. \quad (\text{A17})$$

Similarly, the group multiplication of \mathcal{G}/\mathcal{H} is expressed as

$$\begin{aligned} & g_{i_I} (\mathbf{I}, \mathbf{t}_m) g_{i_J} (\mathbf{I}, \mathbf{t}_n) \mathcal{H} \\ &= g_{i_I} g_{i_J} (\mathbf{I}, \mathbf{R}_{i_J}^{-1} \mathbf{t}_m + \mathbf{t}_n) \mathcal{H} \\ &= (\mathbf{I}, \mathbf{s}(I, J)) g_{i_I i_J} (\mathbf{I}, \mathbf{R}_{i_J}^{-1} \mathbf{t}_m + \mathbf{t}_n) \mathcal{H} \quad (\because \text{Eq. (A16)}) \\ &= g_{i_I i_J} (\mathbf{I}, \mathbf{R}_{i_J}^{-1} \mathbf{t}_m + \mathbf{t}_n + \mathbf{R}_{i_I i_J}^{-1} \mathbf{s}(I, J)) \mathcal{H}. \end{aligned}$$

Finally, we check the associativity condition of \mathcal{G}/\mathcal{H} . For all triplets of coset representatives g_{i_I} , g_{i_J} , and g_{i_K} , we require $(g_{i_I} g_{i_J} \mathcal{H}) g_{i_K} \mathcal{H} = g_{i_I} \mathcal{H} (g_{i_J} g_{i_K} \mathcal{H})$, which leads to the 2-cocycle condition for \mathbf{s} :

$$\begin{aligned} & \mathbf{s}(i_I i_J, i_K) + \mathbf{s}(i_I, i_J) \\ &= \mathbf{s}(i_I, i_J i_K) + \mathbf{R}_{i_I} \mathbf{s}(i_J, i_K) \quad \text{mod } \mathcal{L}_\mathcal{H}. \quad (\text{A18}) \end{aligned}$$

Thus, we obtain a normal k-subgroup \mathcal{H} of \mathcal{M} with $\mathcal{H} \trianglelefteq \mathcal{G}$ by checking Eqs. (A13), (A14), (A15), and (A18). In the following, we denote \mathcal{T}' and \mathcal{L}' as $\mathcal{T}_\mathcal{H}$ and $\mathcal{L}_\mathcal{H}$ for k-subgroup \mathcal{H} , respectively.

4. Injective homomorphism from quotient group to spin rotation quotient group

For each normal subgroup \mathcal{H} of \mathcal{G} , we consider injective homomorphisms $U : \mathcal{G}/\mathcal{H} \rightarrow O(3)/\mathcal{B}_{\text{so}}$. Since the dimension of $\mathcal{B}(\mathcal{X})/\mathcal{B}_{\text{so}}(\mathcal{X})$ is equal to a spin-structure dimension d and every representation in \mathbb{R} can be transformed to an orthogonal representation, U can be regarded as a d -dimensional orthogonal representation of \mathcal{G}/\mathcal{H} . Because two orthogonal representations are equivalent if and only if they are transformed by an orthogonal matrix, the equivalence classes of U as orthogonal representations are identical to those as spin space groups as adopted in Sec. II B. Consequently, it suffices to enumerate the inequivalent injective homomorphisms U by constructing inequivalent d -dimensional faithful orthogonal representations $\tilde{U} : \mathcal{G}/\mathcal{H} \rightarrow O(d)$.

Because orthogonal representations can be uniquely decomposed into irreducible representations in \mathbb{R} (also referred to as physically irreducible representations, PIRs [136]), all \tilde{U} can be constructed by combining PIRs of \mathcal{G}/\mathcal{H} . We numerically enumerate all inequivalent PIRs using SPGREP [137].

After constructing \tilde{U} , we embed its d -dimensional orthogonal matrices into $O(3)$ by direct sum with $(3-d)$ -dimensional identity matrices,

$$U(g_{i_I}(\mathbf{I}, \mathbf{t}_m)\mathcal{H}) = \left(\tilde{U}(g_{i_I}(\mathbf{I}, \mathbf{t}_m)\mathcal{H}) \oplus \mathbf{I}_{3-d} \right) \mathcal{B}_{\text{so}}, \quad (\text{A19})$$

where \mathbf{I}_{3-d} is the $(3-d)$ -dimensional identity matrix.

Appendix B: Symmetry-adapted magnetic moments from projection operator of spin space group

We provide details of the projection operator method to obtain symmetry-adapted magnetic moments $\mathbf{m}^{(\alpha)}$ in Eq. (16) with spin space group \mathcal{X} in Eq. (10) and representation matrices $\mathbf{\Gamma}$ in Eq. (13). Because \mathcal{X} is infinite, we construct the projection operator by decomposing it into those of its subgroups, the spin-only group \mathcal{B}_{so} and the normal space subgroup \mathcal{H} .

We first construct the projection operator for \mathcal{B}_{so} ,

$$\mathbf{P}^{\text{so}} = \int_{\mathbf{U} \in \mathcal{B}_{\text{so}}} \mathbf{U} d\mu(\mathbf{U}), \quad (\text{B1})$$

where $d\mu$ is the normalized Haar measure. For simplicity, we choose the z -axis as the spin axis for collinear and coplanar spin-only groups. Then, the projection operator for a collinear spin-only group is given by

$$\begin{aligned} \mathbf{P}^{\text{so}} &= \frac{1}{2} \left(\mathbf{I} + \begin{pmatrix} -1 & 0 & 0 \\ 0 & 1 & 0 \\ 0 & 0 & 1 \end{pmatrix} \right) \cdot \frac{1}{2\pi} \int_0^{2\pi} \mathbf{U}_\theta^z d\theta \\ &= \begin{pmatrix} 0 & 0 & 0 \\ 0 & 0 & 0 \\ 0 & 0 & 1 \end{pmatrix}, \end{aligned}$$

where \mathbf{U}_θ^z is a rotation matrix around the z -axis by an angle of θ . For a coplanar spin-only group, the projection operator is given by

$$\begin{aligned} \mathbf{P}^{\text{so}} &= \frac{1}{2} \left(\mathbf{I} + \begin{pmatrix} 1 & 0 & 0 \\ 0 & 1 & 0 \\ 0 & 0 & -1 \end{pmatrix} \right) \\ &= \begin{pmatrix} 1 & 0 & 0 \\ 0 & 1 & 0 \\ 0 & 0 & 0 \end{pmatrix}. \end{aligned}$$

For a noncoplanar spin-only group, the projection operator is simply given by $\mathbf{P}^{\text{so}} = \mathbf{I}$.

Next, we construct the projection operator for \mathcal{H} . We denote representatives of inequivalent unit cells under $\mathcal{T}(\mathcal{H})$ as $\ell = \{\ell_1, \dots, \ell_{N_k}\}$. Then, from the periodicity of magnetic moments under $\mathcal{T}(\mathcal{H})$, it suffices to consider unit cells only in ℓ . Thus, we only consider coset representatives of $\mathcal{H}/\mathcal{T}(\mathcal{H})$ in constructing the projection operator,

$$P_{\ell_k, \ell'_{k'}}^{\mathcal{H}} = \frac{1}{|\mathcal{P}(\mathcal{H})|} \sum_{\mathbf{R}_h \in \mathcal{P}(\mathcal{H})} \Gamma_{\ell_k, \ell'_{k'}}^{\text{site}}(g_h). \quad (\text{B2})$$

Finally, we combine the projection operators of \mathcal{B}_{so} and \mathcal{H} to construct that of \mathcal{X} ,

$$P_{\ell_k \mu, \ell'_{k'} \mu'}^{\mathcal{X}} = \frac{1}{N_t N_k} \sum_{I=1}^{N_t} \sum_{m=1}^{N_k} \sum_{\kappa''=1}^m \sum_{\mu''=1}^3 \Gamma_{\ell_k \mu, \ell'_{k'} \kappa'' \mu''}((g_{i_I}(\mathbf{I}, \mathbf{t}_m), \mathbf{U}_{Im})) P_{\ell'_{k''}, \ell'_{k'}}^{\mathcal{H}} P_{\mu'', \mu'}^{\text{so}}. \quad (\text{B3})$$

Eigenvectors of $\mathbf{P}^{\mathcal{X}}$ with eigenvalue 1 give symmetry-adapted magnetic moments $\mathbf{m}^{(\alpha)}$ in Eq. (16).

Appendix C: Orthogonal intertwiner between two orthogonal representations

Let Γ_1 and Γ_2 be orthogonal k -dimensional representations of a finite group G . An intertwiner of Γ_1 and Γ_2

is a non-zero real matrix $\mathbf{Q}' \in \mathbb{R}^{k \times k}$ satisfying

$$\Gamma_1(g)\mathbf{Q}' = \mathbf{Q}'\Gamma_2(g) \quad (\forall g \in G). \quad (\text{C1})$$

The intertwiner exists if and only if Γ_1 and Γ_2 are equivalent.

For any real matrix $\mathbf{B} \in \mathbb{R}^{k \times k}$, the following matrix is an intertwiner for these representations,

$$\mathbf{Q}' := \sum_{g \in G} \Gamma_1(g)\mathbf{B}\Gamma_2(g)^{-1}, \quad (\text{C2})$$

if \mathbf{Q}' is nonzero. Thus, we can construct an intertwiner by generating a random matrix \mathbf{B} and calculating \mathbf{Q}' .

If an intertwiner \mathbf{Q}' exists and is well-conditioned, it can be converted to an orthogonal matrix by

$$\mathbf{Q} = \mathbf{Q}'(\mathbf{Q}'^\top \mathbf{Q}')^{-1/2}, \quad (\text{C3})$$

where $(\mathbf{Q}'^\top \mathbf{Q}')^{-1/2}$ is the inverse square root of the positive definite matrix $\mathbf{Q}'^\top \mathbf{Q}'$.

Appendix D: Spin-planochiral coplanar spin space group

For simplicity, we consider coplanar SSGs \mathcal{X} with $\mathcal{B}_{\text{so}}(\mathcal{X}) = O_{xy}(2) \oplus 1$ without loss of generality. We say that \mathcal{X} is spin-planochiral if \mathcal{X} and $\mathcal{X}_e = (1, \boldsymbol{\sigma}_x)^{-1}\mathcal{X}(1, \boldsymbol{\sigma}_x)$ are not equivalent by any spin transformation $\mathbf{Q} \in SO(2) \oplus 1$, where $\boldsymbol{\sigma}_x$ is a mirror operation perpendicular to the x -axis and is chosen as one of

TABLE IV: Complete list of classifications in Sec. V B. The column “No.” indicates the entries in the MAGNCDATA database. In the “Class” column, Lt, Lp, M, S, and oS correspond to the `lower_family_translation_group`, `lower_family_point_group`, `multiple_basis`, `ssg_matched`, and `oriented_ssg_matched` classes, respectively. Entries marked with an asterisk are used in the SDFT-based analysis shown in Sec. VI.

| No. | Class | No. | Class | No. | Class |
|----------------|-------|-----------------|-------|------------------------|-------|
| 0.1_LaMn03 | oS* | 0.898_Mn3IrSi | M | 1.416_Tb202S | Lp |
| 0.2_Cd20s207 | oS* | 0.899_Mn3IrGe | M | 1.417_Tb202Se | S |
| 0.3_Ca3Li0s06 | oS* | 0.900_Mn3CoGe | M | 1.418_Cu403 | Lp |
| 0.6_YMn03 | oS | 0.903_Pr2PdGe6 | M | 1.419_GdIn3 | Lp |
| 0.7_ScMn03 | oS | 0.904_Nd2PdGe6 | oS | 1.420_YBa2Cu306 | oS* |
| 0.8_ScMn03 | S | 0.905_Tb2PdGe6 | M | 1.421_NdRh2Si2 | oS |
| 0.9_GdB4 | oS | 0.906_Dy2PdGe6 | M | 1.422_ErRh2Si2 | oS |
| 0.12_U3Ru4Al12 | M | 0.907_Ho2PdGe6 | M | 1.423_UPb3 | Lp |
| 0.15_MnF2 | oS* | 0.908_Tb2PtGe6 | M | 1.424_UCu5 | Lp |
| 0.16_EuTi03 | oS | 0.909_Er2PtGe6 | oS | 1.425_UGeTe | oS |
| 0.17_FePO4 | M | 0.910_TbNiSi2 | oS | 1.426_UGeS | oS |
| 0.18_BaMn2As2 | oS* | 0.916_Cd20s207 | oS | 1.427_HoCo2Ge2 | oS |
| 0.19_MnTi03 | oS* | 0.917_Sr2Sc0s06 | S* | 1.428_UN | Lp |
| 0.20_MnTe2 | oS* | 0.918_Ag2Ru04 | M | 1.432_Ba2LuRu06 | Lp |
| 0.21_PbNi03 | oS* | 0.919_EuMnBi2 | oS | 1.433_Ba2YRu06 | Lp |
| 0.22_DyB4 | Lp | 0.920_ThMnPN | oS* | 1.438_BaCoF4 | Lp |
| 0.23_Ca3Mn207 | oS* | 0.921_ThMnPN | oS | 1.439_BaCoF4 | Lt |
| 0.24_LiMnPO4 | oS* | 0.922_ThMnAsN | oS* | 1.441_NaFe3(SO4)2(OH)6 | oS |
| 0.25_Na0s03 | oS* | 0.923_ThMnAsN | oS | 1.442_URu2Si2 | oS |
| 0.28_LiFeSi206 | M | 0.924_RbRu04 | M | 1.445_Y2BaCu05 | Lp |

improper spin rotations out of the coplanar plane. We denote the triplets of \mathcal{X} and \mathcal{X}_e , defined in Sec. II B as $(\mathcal{H}, \mathcal{B}_{\text{so}}, U)$ and $(\mathcal{H}, \mathcal{B}_{\text{so}}, U_e)$, respectively. We write the corresponding two-dimensional faithful orthogonal representations for U and U_e , defined in Appendix A 4, as \tilde{U} and \tilde{U}_e , respectively. Then, \mathcal{X} is spin-planochiral if there is no orientation-preserving intertwiner $\tilde{\mathbf{Q}} \in SO(2)$ between \tilde{U} and \tilde{U}_e .

This condition requires both (1) \tilde{U} and \tilde{U}_e are $O(2)$ -equivalent and (2) a centralizer of \tilde{U} has an improper rotation. The first condition can be checked by the procedure in Appendix C. The second condition is satisfied if and only if \tilde{U} is a two-dimensional PIR as follows. Otherwise, \tilde{U} is constructed from two one-dimensional PIRs, u_1 and u_2 , as $\tilde{U} = u_1 \oplus u_2$ after some transformation. We can construct improper $\tilde{\mathbf{Q}} = \text{diag}(-1, 1)$ as a centralizer of \tilde{U} by flipping the axis of u_1 . Thus, \tilde{U} must be a two-dimensional PIR if \mathcal{X} is spin-planochiral.

Appendix E: Complete list of classifications

We present the complete list of classifications in Table IV. Details of the classification scheme and remarks are provided in Sec. V A. The entries used in the SDFT-based analysis in Sec. VI are also indicated.

TABLE IV (*cont.*)

| No. | Class | No. | Class | No. | Class |
|---------------------|-------|----------------------------|-------|--------------------------|-------|
| 0.29_Er2Ti207 | M | 0.926_Pr2PdGe6 | M | 1.446_CeCoAl4 | oS |
| 0.30_YbMn03 | oS | 0.927_Nd2PdGe6 | oS | 1.448_HoSi | Lt |
| 0.31_HoMn03 | oS | 0.928_Dy2PdGe6 | M | 1.449_Li2CuW208 | S* |
| 0.32_HoMn03 | oS | 0.929_Tb2PdGe6 | M | 1.452_FeSn | oS* |
| 0.44_YMn03 | S | 0.930_Ho2PdGe6 | M | 1.453_EuMn2Si2 | oS* |
| 0.45_La2Ni04 | Lp | 0.931_Tb2PtGe6 | M | 1.454_Mn6Ni16Si7 | Lp |
| 0.47_Gd2Sn207 | Lp | 0.932_Er2PtGe6 | oS | 1.455_Mn6Ni16Si7 | M |
| 0.50_MnTi03 | oS | 0.934_Sr2NiTe06 | S* | 1.456_Sr2Cu02Cu2S2 | oS |
| 0.56_Ba2CoGe207 | oS* | 0.936_Sr2MnTe06 | S* | 1.457_NdNiMg15 | Lp |
| 0.58_CoAl204 | oS* | 0.937_Sr2CoTe06 | S | 1.458_CsCo2Se2 | oS* |
| 0.59_Cr203 | oS* | 0.942_Er2Ge207 | M | 1.460_PrCuSi | Lp |
| 0.62_SrMn2V208 | oS | 0.945_Yb2Ir207 | oS* | 1.461_Sr2Cr3As202 | oS* |
| 0.65_Fe203-alpha | oS* | 0.947_YCr03 | oS | 1.462_La2CoPt06 | S |
| 0.66_Fe203-alpha | S | 0.950_LaEr03 | M | 1.463_Sr2Fe3Se203 | M |
| 0.70_Na3Co(CO3)2Cl | oS | 0.955_Na2Mn(H2C3O4)2(H2O)2 | oS | 1.464_U2N2P | oS |
| 0.71_Li2Ni(SO4)2 | oS | 0.959_Cr2Te06 | oS | 1.465_U2N2As | oS |
| 0.72_CaMnBi2 | oS* | 0.960_Fe2Te06 | oS | 1.468_TbMn2Si2 | oS* |
| 0.73_SrMnBi2 | oS* | 0.961_LiCrGe206 | S | 1.469_YMn2Si2 | oS* |
| 0.74_Mn3Cu0.5Ge0.5N | oS* | 0.962_LiCrGe206 | S | 1.470_UCr2Si2 | S |
| 0.75_Cr2W06 | oS* | 0.963_LiCrGe206 | S | 1.471_EuCd2As2 | oS |
| 0.76_Cr2Te06 | oS* | 0.964_LiCrGe206 | S | 1.472_CaOFeS | Lp |
| 0.79_CaIr03 | oS* | 0.966_V2W06 | oS* | 1.473_CuBr(C4H4N2)2(BF4) | oS |
| 0.80_U2Pd2In | oS | 0.967_BaMn2V208 | oS | 1.474_CuCl(C4H4N2)2(BF4) | oS |
| 0.81_U2Pd2Sn | oS | 0.979_TmV03 | oS* | 1.475_DyNiAl4 | oS |
| 0.83_LiFeP207 | S* | 0.980_TmV03 | oS | 1.476_Ba2Co04 | M |
| 0.87_NaFeP04 | oS* | 0.984_LuV03 | oS* | 1.477_Ba2Co04 | M |
| 0.88_LiNiP04 | M | 0.987_BaFe2S20 | M | 1.478_CoTi205 | Lp |
| 0.89_BaMn2Bi2 | oS* | 0.988_BaFe2Se20 | M | 1.479_U2Ni2Sn | oS |
| 0.92_CaMn2Sb2 | oS* | 0.991_HoFe03 | oS* | 1.482_Er2Fe2Si2C | Lp |
| 0.95_LiFeP04 | oS* | 0.1004_Cs02 | M | 1.484_Li2MnGe04 | M |
| 0.96_CoSO4 | M | 0.1005_Mn3RhGe | M | 1.486_CeRhAl4Si2 | oS |
| 0.97_FeSb204 | M | 0.1006_Mn3IrGe | M | 1.487_CeIrAl4Si2 | oS |
| 0.104_ErV03 | M | 0.1010_C10H6MnN404 | M | 1.488_CeMn2Si2 | oS* |
| 0.107_Ho2Ge207 | M | 0.1015_CoTe6013 | oS | 1.489_CeMn2Si2 | oS |
| 0.108_Mn3Ir | oS* | 0.1017_CePdAl3 | oS | 1.490_CeMn2Si2 | oS |
| 0.109_Mn3Pt | oS* | 0.1018_SrMn03 | oS* | 1.491_PrMn2Si2 | oS* |
| 0.110_Cr203 | oS | 0.1019_SrMn03 | oS | 1.492_PrMn2Si2 | oS |
| 0.112_FeB03 | oS* | 0.1020_EuCu2Sb2 | oS | 1.493_NdMn2Si2 | oS* |
| 0.113_NiC03 | S* | 0.1021_TmFe03 | oS* | 1.494_NdMn2Si2 | oS |
| 0.114_CoC03 | S* | 0.1022_TmFe03 | oS | 1.495_YMn2Si2 | oS |
| 0.115_MnC03 | S* | 0.1023_Cr2Mo06 | oS* | 1.496_YMn2Ge2 | oS* |
| 0.116_FeC03 | oS* | 0.1036_CoTa4Se8 | oS* | 1.497_EuMg2Bi2 | oS |
| 0.117_LuFe03 | oS | 0.1059_PrBaMn206 | oS* | 1.498_Cu6(SiO3)6(H2O)6 | M |
| 0.119_CoSe205 | M | 0.1064_RuP3Si011 | oS | 1.499_CsFe(MoO4)2 | S |
| 0.122_Li2Mn(SO4)2 | M | 0.1065_MnGeN2 | oS* | 1.504_GdCuSn | Lp |
| 0.125_MnGe03 | oS* | 0.1066_MnSiN2 | oS* | 1.505_GdAgSn | Lp |
| 0.126_NpCo2 | oS | 0.1076_Li2Ni2W209 | M | 1.506_GdAuSn | Lp |
| 0.127_Dy3Al5012 | oS | 0.1078_[Na(OH2)3]Mn(NCS)3 | oS | 1.507_NdPd5Al2 | Lt |
| 0.128_FeS04F | oS* | 0.1081_Mn2Au | oS | 1.508_Mn2AlB2 | oS* |
| 0.131_Mn(N(CN2))2 | oS* | 0.1082_LuCrW06 | oS | 1.510_TbNi2Ge2 | Lt |
| 0.137_Cu2V207 | oS* | 0.1083_RuP3Si011 | oS | 1.511_TbNi2Si2 | Lp |
| 0.142_Fe2Te06 | oS* | 0.1085_PrFe03 | oS* | 1.512_TbCo2Si2 | oS |
| 0.143_Cr2Te06 | oS | 0.1090_NH4CrF3 | oS | 1.513_HoCo2Si2 | oS |
| 0.144_Cr2W06 | oS | 0.1091_La203Mn2Se2 | oS* | 1.514_HoCo2Si2 | oS |
| 0.146_EuZr03 | oS | 0.1092_La203Mn2Se2 | oS | 1.515_ErCo2Si2 | S |
| 0.147_EuZr03 | oS | 0.1093_La203Mn2Se2 | oS | 1.516_ErCo2Si2 | oS |
| 0.148_La2LiRu06 | S* | 0.1103_EuSc2Te4 | oS | 1.519_CoSO4 | M |
| 0.150_NiS2 | oS* | 0.1104_GdCr03 | oS* | 1.520_NiSO4 | oS* |
| 0.152_LiFeP04 | M | 0.1111_MnSb204 | oS* | 1.521_FeSO4 | oS* |
| 0.155_CaMnGe206 | S | 0.1112_CoNb4Se8 | oS* | 1.522_CrV04 | S* |

TABLE IV (*cont.*)

| No. | Class | No. | Class | No. | Class |
|--------------------------|-------|----------------------|-------|-------------------|-------|
| 0.156_CaMnGe206 | S* | 1.0.1_Ag2Cr02 | Lt | 1.523_VP04 | Lt |
| 0.159_DyCo03 | M | 1.0.8_Ba3MnNb209 | oS | 1.524_InMn03 | M |
| 0.160_TbCo03 | M | 1.0.9_CsCoCl3 | Lt | 1.525_InMn03 | M |
| 0.161_CoSe205 | oS | 1.0.14_CsFeCl3 | oS | 1.526_LiCoF4 | S* |
| 0.163_MnPS3 | S* | 1.0.26_RbCoBr3 | Lt | 1.527_CsNiF3 | Lp |
| 0.171_DySc03 | M | 1.0.27_Li2MnTe06 | Lt | 1.530_CeC2 | oS |
| 0.177_Mn3GaN | oS* | 1.0.32_EuIn2As2 | oS | 1.531_PrC2 | oS |
| 0.178_CoF2 | oS* | 1.0.33_FeF3 | M | 1.532_NdC2 | oS |
| 0.180_MnPSe3 | S* | 1.0.36_CsMnI3 | Lt | 1.533_TbC2 | Lt |
| 0.186_CeMnAs0 | oS* | 1.0.37_CsMnI3 | Lt | 1.534_HoC2 | Lt |
| 0.189_CeMn2Ge4012 | oS | 1.0.38_CsCoCl3 | Lt | 1.535_UPd2Ge2 | Lt |
| 0.193_LiCoP04 | oS* | 1.0.42_CsNiCl3 | oS | 1.536_UPd2Si2 | oS |
| 0.194_UPt2Si2 | oS | 1.0.45_Ba3CoSb209 | oS | 1.537_URh2Si2 | oS |
| 0.198_GdV04 | oS | 1.0.58_Li2MnTe06 | oS | 1.538_Ba2MnTe06 | S* |
| 0.199_Mn3Sn | oS* | 1.1_Mn304 | oS | 1.539_KMnP | oS* |
| 0.200_Mn3Sn | oS | 1.2_CuSe205 | M | 1.540_KMnP | oS |
| 0.207_T1Fe1.6Se2 | M | 1.3_Sr2Ir04 | Lp | 1.541_RbMnP | oS* |
| 0.208_T1Fe1.6Se2 | S | 1.4_YBa2Cu306+d | oS | 1.542_RbMnP | oS |
| 0.209_T1Fe1.6Se2 | oS* | 1.5_YBa2Cu306+d | oS* | 1.543_RbMnAs | oS* |
| 0.211_Ca2Mn04 | oS* | 1.6_Ni0 | Lp | 1.544_RbMnAs | oS |
| 0.212_Sr2Mn3As202 | oS* | 1.8_CeRu2Al10 | oS | 1.545_RbMnBi | oS* |
| 0.215_BaNi2P208 | S* | 1.9_Li2V0Si04 | Lp | 1.546_CsMnBi | oS* |
| 0.216_SrEr204 | oS | 1.13_Ba3Nb2Ni09 | oS | 1.547_CsMnP | oS* |
| 0.217_LiCrGe206 | S | 1.16_BaFe2As2 | oS* | 1.548_CsMnP | oS |
| 0.222_CuMnAs | oS* | 1.17_CoV206-alpha | S* | 1.549_U2Ni2In | oS |
| 0.229_Ba2MnSi207 | oS* | 1.18_MnS2 | oS* | 1.550_LiMnAs | oS* |
| 0.230_K2CoP207 | oS | 1.20_HoMn03 | Lp | 1.551_LiMnAs | oS |
| 0.236_CaFe4Al8 | M | 1.21_DyCo2Si2 | oS | 1.552_LiMnAs | oS |
| 0.237_Er2Sn207 | Lp | 1.22_DyCu2Si2 | Lp | 1.553_KMnAs | oS* |
| 0.238_Er2Pt207 | Lp | 1.23_La2Cu04 | oS* | 1.554_KMnAs | oS |
| 0.239_Ca3LiRu06 | oS* | 1.24_ZnV204 | Lp | 1.556_FeSn2 | oS* |
| 0.243_Li2Fe(SO4)2 | S | 1.25_KFe3(OH)6(SO4)2 | oS | 1.557_FeGe2 | oS* |
| 0.244_Li2Co(SO4)2 | oS | 1.26_CsFe2Se3 | Lp | 1.558_MnSn2 | Lp |
| 0.246_LiFe(SO4)2 | oS | 1.28_CrN | Lt | 1.559_MnSn2 | Lt |
| 0.252_Cs2FeCl5.D20 | oS | 1.30_BaCo2V208 | Lp | 1.560_GeNi204 | Lp |
| 0.254_[C(ND2)3]Cu(DCOO)3 | oS | 1.31_Mn0 | Lp | 1.561_GeNi204 | M |
| 0.255_[C(ND2)3]Cu(DCOO)3 | oS | 1.33_ErAuGe | Lp | 1.562_GeNi204 | M |
| 0.264_Fe3(P04)2 | S* | 1.34_HoAuGe | M | 1.563_GeNi204 | M |
| 0.267_YbMnBi2 | oS* | 1.35_LiErF4 | Lp | 1.564_GeCo204 | M |
| 0.273_Mn3ZnN | oS* | 1.37_VOCl | S* | 1.568_GdCu2Si2 | Lp |
| 0.277_MgMn03 | oS* | 1.39_LiFeGe206 | M | 1.569_SrRu206 | oS |
| 0.279_Mn3As | oS* | 1.42_La2Ni04 | oS* | 1.570_La30s07 | Lp |
| 0.280_Mn3As | oS | 1.43_PrNi03 | Lp | 1.571_La30s07 | Lp |
| 0.284_K0s04 | oS* | 1.45_NdNi03 | Lp | 1.573_FeS04 | M |
| 0.285_KRu04 | oS* | 1.49_Ag2Ni02 | Lt | 1.574_NdBiPt | Lp |
| 0.290_CeCu2 | oS | 1.50_AgNi02 | Lp | 1.575_ErRh | Lp |
| 0.292_NiTe205 | M | 1.52_CaFe2As2 | oS* | 1.576_Yb202S | oS |
| 0.301_Sr2CoTe06 | S* | 1.56_Gd2Ti207 | oS | 1.578_KErSe2 | Lp |
| 0.303_BaCrF5 | oS* | 1.57_CuMn02 | S* | 1.580_NiTi03 | S* |
| 0.307_ScCr03 | oS* | 1.58_La202Fe20Se2 | M | 1.585_PrFeAs0 | oS* |
| 0.308_InCr03 | oS* | 1.59_KTb3F12 | oS | 1.588_NdFeAs0 | oS* |
| 0.309_T1Cr03 | oS* | 1.60_Ca3Co206 | Lp | 1.593_BaCoSO | Lt |
| 0.315_ZrMn2Ge4012 | oS | 1.61_MnW04 | Lt | 1.594_BaCoSO | Lt |
| 0.320_U2Pd2In | oS | 1.62_Cu0 | Lt | 1.595_CaCoSO | Lt |
| 0.321_U2Pd2Sn | oS | 1.63_MnPb4Sb6S14 | oS | 1.596_TbCuSb2 | Lp |
| 0.323_LaCr03 | oS | 1.64_BaNiF4 | Lp | 1.597_TbCuSb2 | Lt |
| 0.324_CdYb2S4 | Lp | 1.65_SrFe02 | oS* | 1.617_LiFe(Mo04)2 | S |
| 0.325_CdYb2Se4 | Lp | 1.66_Fe(ND3)2P04 | M | 1.618_Co0 | Lp |
| 0.326_Nd2Sn207 | oS | 1.69_Co0 | S* | 1.619_MnS | Lp |
| 0.330_ErGe3 | S | 1.70_CoV206 | S* | 1.620_NdCu2 | Lt |

TABLE IV (*cont.*)

| No. | Class | No. | Class | No. | Class |
|--------------------|-------|------------------------|-------|------------------------|-------|
| 0.334_CoF3 | oS* | 1.71_SrCo2V208 | M | 1.623_EuMg2Bi2 | oS |
| 0.335_FeF3 | oS* | 1.77_Sr2Ir04 | M | 1.624_EuSn2P2 | oS |
| 0.336_NdFe03 | oS* | 1.79_Li2CoSi04 | M | 1.625_Sr2Fe3S203 | oS |
| 0.339_Nd2Hf207 | oS | 1.80_Dy2CoGa8 | oS | 1.627_KCeS2 | Lp |
| 0.340_Nd2Zr207 | oS | 1.81_GdIn3 | Lp | 1.629_FeGe | oS* |
| 0.345_Tb2C3 | Lp | 1.82_Nd2RhIn8 | oS | 1.630_LuMn6Sn6 | oS* |
| 0.348_Bi2Cu04 | oS* | 1.87_Tb2CoGa8 | oS | 1.631_YMn6Ge6 | oS* |
| 0.350_TbAl03 | M | 1.88_Mn5Si3 | M | 1.635_ErFe2Si2 | Lt |
| 0.351_TbFe03 | oS* | 1.94_Ba3LaRu209 | Lp | 1.636_ErMn2Si2 | oS* |
| 0.354_TbCr03 | oS* | 1.95_BaNd204 | M | 1.637_ErMn2Si2 | oS |
| 0.361_Sr3LiRu06 | oS* | 1.96_BaNd204 | M | 1.638_ErMn2Ge2 | oS* |
| 0.362_RbFeC15(D20) | oS | 1.97_Li2Mn03 | S* | 1.639_ErMn2Ge2 | oS |
| 0.363_KFeC15(D20) | oS | 1.99_CsCoC13(D20)2 | M | 1.640_ErMn2Ge2 | oS |
| 0.364_SrCr2As2 | oS* | 1.100_Cu2MnSnS4 | Lp | 1.641_Ba2FeSi207 | oS |
| 0.365_BaCr2As2 | oS* | 1.101_LuMn03 | Lp | 1.642_TlFeS2 | S* |
| 0.377_Mn3Ge | oS* | 1.103_U2Rh2Sn | oS | 1.643_Dy0Cl | oS |
| 0.378_UBi2 | oS | 1.104_Gd2Cu04 | Lp | 1.644_EuSn2As2 | oS |
| 0.379_SmFe03 | oS* | 1.107_Sm2Cu04 | Lp | 1.648_Nd203 | Lp |
| 0.380_SmFe03 | oS | 1.110_ScMn6Ge6 | oS* | 1.649_Sr3ZnIr06 | M |
| 0.382_LiMnP04 | oS | 1.111_GdBiPt | Lp | 1.653_FeW04 | S* |
| 0.383_LiCoP04 | oS | 1.112_NiTa206 | Lt | 1.654_NiNb206 | M |
| 0.384_LiCoP04 | S | 1.113_NiSb206 | Lp | 1.655_FeNb206 | M |
| 0.385_LiCoP04 | M | 1.114_Ca4Ir06 | M | 1.656_CoNb206 | Lp |
| 0.388_Co3Al2Si3012 | M | 1.115_Dy3Ru4Al12 | M | 1.659_MnCl2(CO(NH2)2)2 | oS |
| 0.398_Ca2Ru04 | M | 1.116_AgMnV04 | M | 1.660_FePb4Sb6S14 | M |
| 0.399_FeOOH | oS* | 1.117_NaFeP04 | M | 1.663_Tb2Ni2In | Lp |
| 0.401_Sr4Fe4011 | oS* | 1.118_GdP04 | M | 1.664_DyV04 | Lp |
| 0.402_Sr4Fe4011 | oS | 1.120_BaFe2Se3 | M | 1.665_Ba3CoNb209 | oS |
| 0.404_Sr3NaRu06 | oS* | 1.121_NaFeS04F | S | 1.666_TbCoGa5 | Lp |
| 0.406_GdNiSi3 | oS | 1.125_LaFeAs0 | oS* | 1.667_UPtGa5 | Lp |
| 0.410_GdAl03 | oS | 1.126_NaCoS04F | M | 1.668_HoCoGa5 | Lp |
| 0.413_UGeSe | oS | 1.127_BiNi0(P04) | M | 1.669_KFe(P03F)2 | M |
| 0.416_LaCr03 | oS* | 1.128_BiCo0(P04) | M | 1.671_NpCoGa5 | oS |
| 0.417_LaCr03 | oS | 1.129_AgFe3(S04)2(0D)6 | oS | 1.672_EuZn2As2 | oS |
| 0.419_ErGe207 | M | 1.133_CuSb206 | M | 1.673_EuCd2Sb2 | oS |
| 0.420_Sr2LuRu06 | S* | 1.134_Co2C1008H2 | S | 1.678_CrN | oS* |
| 0.421_EuMnSb2 | oS* | 1.136_AgCrS2 | Lt | 1.681_PrFe2A18 | M |
| 0.423_EuMnSb2 | oS | 1.138_MgV204 | M | 1.683_UPdGa5 | oS |
| 0.426_EuMnBi2 | oS* | 1.139_Ho2RhIn8 | Lp | 1.685_NiCr204 | Lp |
| 0.427_Sm2Ti207 | oS | 1.140_PrMgPb | S | 1.689_LuMn2Ge2 | oS* |
| 0.430_Yb3Pt4 | M | 1.141_NdMgPb | S | 1.690_TmMn2Ge2 | oS* |
| 0.432_KMnF3 | oS | 1.142_CeMgPb | Lp | 1.691_YMn2Ge2 | oS |
| 0.433_KMnF3 | oS* | 1.143_Mn3Pt | Lp | 1.692_YMn2Ge2 | oS |
| 0.434_K2ReI6 | S* | 1.144_NH4FeCl2(HCOO) | S | 1.694_TbMn2Ge2 | oS* |
| 0.440_SrCuTe206 | oS | 1.145_Mn3Ni20P6 | Lp | 1.695_Mn3Ni2Si | M |
| 0.444_YbCl3 | S | 1.146_LaCrAs0 | oS* | 1.696_HoNiSi2 | oS |
| 0.448_Ce4Ge3 | Lp | 1.147_Li2Fe(S04)2 | M | 1.699_GdInCu4 | Lt |
| 0.451_DyRuAs0 | oS | 1.150_PrAg | Lp | 1.700_HoInCu4 | oS |
| 0.452_TbRuAs0 | oS | 1.153_Mn3GaC | Lp | 1.701_HoCdCu4 | Lp |
| 0.453_DyCoSi2 | oS | 1.154_NaFeSi206 | S | 1.702_YBaCo205 | oS* |
| 0.454_PrScSb | oS | 1.158_YMn3A14012 | oS | 1.706_Ba2MnTe06 | Lp |
| 0.461_CoRh204 | oS* | 1.159_Li2Ni(W04)2 | S* | 1.707_Ba2MnW06 | Lp |
| 0.462_MnAl204 | oS* | 1.160_UP | Lp | 1.709_CsCrF4 | M |
| 0.463_Co3O4 | oS* | 1.162_NdMg | Lp | 1.714_CeAuBi2 | oS |
| 0.464_BaMn2P2 | oS* | 1.163_TmPdIn | Lt | 1.715_Sr2CoW06 | S |
| 0.465_HoCr2Si2 | oS* | 1.166_La2Li0s06 | M | 1.716_Sr2MnMo06 | M |
| 0.466_ThCr2Si2 | oS* | 1.167_NiS2 | M | 1.717_Sr2MnW06 | M |
| 0.467_TbP04 | oS | 1.168_Sr2CuTe06 | Lp | 1.718_Ca2MnW06 | M |
| 0.468_ErB4 | Lp | 1.169_CaCoGe206 | S | 1.719_Ca2MnW06 | M |
| 0.469_TbB4 | Lp | 1.171_Tb2Fe2Si2C | oS | 1.721_UCu5 | Lp |

TABLE IV (cont.)

| No. | Class | No. | Class | No. | Class |
|-----------------------|-------|------------------------|-------|----------------------|-------|
| 0.470_BaMn2Sb2 | oS* | 1.172_NiTa206 | Lt | 1.722_Ba3LaRu209 | Lp |
| 0.471_Ba2Mn3Sb202 | oS* | 1.176_YbCo2Si2 | Lt | 1.723_NaMn204 | M |
| 0.472_LaMn2Si2 | oS* | 1.177_Sr2CuW06 | Lp | 1.724_Ba2NiTe06 | Lp |
| 0.474_EuMn2Ge2 | oS* | 1.180_Na3Co2Sb06 | Lp | 1.725_Ba3NiTa209 | oS |
| 0.475_Sr2TbIr06 | S | 1.183_FePS3 | S* | 1.727_Tm3Cu4Ge4 | Lt |
| 0.476_Cs2[FeCl5(H2O)] | oS | 1.185_GeCu204 | Lp | 1.728_Tm3Cu4Sn4 | oS |
| 0.482_SrMn2As2 | oS* | 1.186_SrRu206 | oS* | 1.729_Gd2Fe2Si2C | oS |
| 0.483_YbMn2Sb2 | S* | 1.187_TbRh2Si2 | oS | 1.730_Cu2MnSiS4 | M |
| 0.484_U2N2S | oS | 1.188_CeRh2Si2 | Lp | 1.731_Cu2FeSiS4 | M |
| 0.485_U2N2Se | oS | 1.189_TbMg3 | Lp | 1.732_Cu2MnSnS4 | Lp |
| 0.486_ErCr2Si2 | oS* | 1.190_YCr(B03)2 | S* | 1.733_Cu2MnGeS4 | M |
| 0.491_NdB4 | S | 1.191_HoCr(B03)2 | S* | 1.734_Cu2FeGeS4 | Lp |
| 0.492_NdB4 | M | 1.194_NiW04 | S* | 1.735_Li2FeGeS4 | oS |
| 0.498_LaMn2Si2 | oS | 1.195_Er2Ni2In | Lt | 1.736_Mn(NH5)2(SO4)2 | S |
| 0.499_UCr2Si2C | oS* | 1.196_MnV206 | M | 1.738_TbNiAl | M |
| 0.501_LiFe2F6 | oS* | 1.197_Fe4Si2Sn7016 | M | 1.740_CeAuSb2 | Lt |
| 0.504_NaCrSi206 | S* | 1.199_Sc2NiMn06 | S | 1.741_KNiAs04 | S* |
| 0.505_Pb2VO(P04)2 | oS | 1.200_U2Ni2Sn | oS | 1.742_KNiAs04 | Lp |
| 0.513_YRu03 | oS* | 1.205_Dy2Fe2Si2C | oS | 1.743_CeRhGe3 | Lt |
| 0.518_TbCr2Si2 | oS* | 1.206_Dy2Fe2Si2C | S | 1.744_PrPdSn | Lp |
| 0.519_HoCr2Si2 | oS | 1.208_UAs | Lp | 1.746_YMn2 | Lp |
| 0.520_TbCo03 | M | 1.210_FePS3 | Lp | 1.747_ErAuIn | oS |
| 0.521_DyCo03 | M | 1.211_Dy202S | Lp | 1.749_HoSbTe | Lp |
| 0.523_CaMn2Sb2 | S | 1.212_Dy202Se | Lp | 1.750_HoSbTe | Lt |
| 0.524_MnPSe3 | S | 1.213_Ho202Se | Lp | 1.751_CaCo3Ti4012 | Lt |
| 0.527_Er2Si207 | S | 1.214_Yb202Se | S | 1.753_HoBi | Lp |
| 0.528_CrSb | oS* | 1.215_UP2 | oS | 1.755_KErSe2 | Lp |
| 0.530_SrCuTe206 | oS | 1.219_CuF2 | S* | 1.757_Pr2PdAl7Ge4 | M |
| 0.552_Pb2Mn04 | M | 1.222_Er2CoGa8 | Lp | 1.758_CaMn3V4012 | M |
| 0.553_K2ReI6 | S | 1.223_Tm2CoGa8 | Lp | 1.759_ZnFe204 | Lt |
| 0.562_Ce2Ni3Ge5 | oS | 1.224_CoNb206 | M | 1.760_ZnFe204 | Lp |
| 0.563_Ce2Ni3Ge5 | oS | 1.225_ScMn6Ge6 | oS | 1.761_ZnFe204 | Lt |
| 0.564_U2Rh3Si5 | M | 1.226_CeCo2Ge4012 | M | 1.763_BaNiTe207 | M |
| 0.565_Ce2Ni3Ge5 | M | 1.228_RuCl3 | S | 1.764_NdSbTe | Lt |
| 0.566_TbNiGe2 | oS | 1.229_BaMoP208 | Lp | 1.765_DySbTe | oS |
| 0.571_CoS04 | M | 1.230_NiPS3 | S* | 1.767_Li2CoCl14 | oS* |
| 0.575_ZnFeF5(H2O)2 | oS* | 1.232_CuMnSb | Lp | 1.769_Ni2Te308 | M |
| 0.581_FeF3 | oS | 1.233_CuMnSb | Lp | 1.770_Tb2Ni2In | Lp |
| 0.582_Fe3F8(H2O)2 | oS* | 1.235_Ba(TiO)Cu4(P04)4 | M | 1.772_Pr2PdAl7Ge4 | M |
| 0.585_YbCl3 | S | 1.237_VC12 | oS* | 1.773_PrIr3B2 | Lp |
| 0.586_YCr03 | oS* | 1.238_VBr2 | oS* | 1.774_BaNd2Pt05 | M |
| 0.587_TmCr03 | oS* | 1.239_MnBr2 | Lt | 1.775_CaCu3Ti4012 | M |
| 0.591_ErCr03 | oS* | 1.240_FeI2 | Lt | 1.777_EuAl2Si2 | oS |
| 0.592_DyCr03 | oS* | 1.241_FeCl2 | oS* | 1.778_ThCr2Si2C | oS* |
| 0.598_AlCr2 | S* | 1.242_FeBr2 | oS* | 1.782_FeBr3 | oS* |
| 0.599_CaMnSi | oS* | 1.244_CrCl3 | S* | 1.784_Li2CoCl14 | oS |
| 0.600_CaMnSi | oS | 1.245_CoBr2 | S* | 1.785_K2ReCl6 | M |
| 0.601_CaMnGe | S* | 1.246_CoCl2 | S* | 1.786_RuBr3 | Lp |
| 0.602_CaMnGe | S | 1.247_NiCl2 | S* | 1.787_RuCl3 | Lp |
| 0.603_CaMn2Ge2 | oS* | 1.248_NiBr2 | S* | 1.793_Ca3Ru207 | oS |
| 0.604_CaMn2Ge2 | oS | 1.249_K2NiF4 | Lp | 1.794_Ca3Ru207 | oS |
| 0.605_BaMn2Ge2 | oS* | 1.250_KNiF3 | oS* | 1.795_BiMn3Cr4012 | oS |
| 0.606_BaMn2Ge2 | oS | 1.252_CaCo2P2 | oS* | 1.796_BiMn3Cr4012 | oS |
| 0.607_Ru02 | oS* | 1.253_CeCo2P2 | oS* | 1.799_Mn0 | S* |
| 0.608_PrMn03 | oS* | 1.254_UNiGa5 | oS | 1.800_Ni0 | Lp |
| 0.609_NdMn03 | S* | 1.255_UPtGa5 | oS | 1.802_CrSBr | oS* |
| 0.611_BaMnSb2 | oS* | 1.256_BaNi2V208 | S* | 1.803_LiCrTe2 | oS* |
| 0.617_KMnSb | oS* | 1.257_BaNi2As208 | Lp | 1.805_FeVMo07 | S |
| 0.618_KMnBi | oS* | 1.260_NaMnGe206 | Lp | 1.806_CrVMo07 | S |
| 0.619_LaMnAs0 | oS* | 1.261_NpRhGa5 | oS | 1.807_FeW04 | S |

TABLE IV (*cont.*)

| No. | Class | No. | Class | No. | Class |
|-------------------|-------|-------------------------|-------|-----------------------------|-------|
| 0.620_NdMnAs0 | oS* | 1.262_NpRhGa5 | oS | 1.809_BiCo03 | oS* |
| 0.623_NdMnAs0 | oS | 1.263_Ca3Ru207 | oS | 1.810_BiCo03 | oS |
| 0.624_LaMnAs0 | oS | 1.264_CoPS3 | S* | 1.811_BiCo03 | oS |
| 0.625_U2Pd2In | oS | 1.265_CuMnSb | Lp | 1.821_Yb3Ga5012 | M |
| 0.626_NaMnP | oS* | 1.267_Dy2Co3Al9 | M | 1.822_Sr2MnSi207 | M |
| 0.627_NaMnP | oS | 1.271_CeSbTe | oS | 1.823_Sr2MnSi207 | M |
| 0.628_NaMnP | oS | 1.272_CeNiAs0 | M | 1.824_PbCo2V208 | M |
| 0.629_NaMnAs | oS* | 1.278_Cu(NCS)2 | S* | 1.826_NdZnPO | Lp |
| 0.630_NaMnAs | oS | 1.281_YBaCuFe05 | oS* | 1.828_ZnFe204 | Lt |
| 0.631_NaMnSb | oS* | 1.286_Fe2(C204)3.4H20 | S | 1.830_FeBi4S7 | oS* |
| 0.632_NaMnSb | oS | 1.287_V203 | S* | 1.833_Pb(OF)Cu3(Se03)2(N03) | M |
| 0.633_KFeS2 | S* | 1.288_CePd2Si2 | Lp | 1.834_Na3Co(C03)2Cl | oS |
| 0.634_NaMnBi | oS* | 1.289_CePd2Ge2 | Lp | 1.835_La2Co203Se2 | M |
| 0.635_NaMnBi | oS | 1.290_CeRh2Si2 | Lp | 1.838_LaMn2Au4 | oS* |
| 0.636_RbFeS2 | S* | 1.291_CeAu2Si2 | oS | 1.840_Sr2Mn205 | M |
| 0.637_KFeSe2 | oS* | 1.292_HoNi2B2C | oS | 1.841_Sr3Fe205Cl2 | Lp |
| 0.638_RbFeSe2 | oS* | 1.293_NdNi2B2C | Lp | 1.842_Ca2Fe03Cl | oS |
| 0.639_Mn2Au | oS* | 1.294_HoNi2B2C | oS | 1.843_Ca2Fe03Cl | oS |
| 0.640_Mn2Au | oS | 1.295_DyNi2B2C | oS | 1.844_Sr2Fe03Cl | oS |
| 0.642_LaMn03 | oS | 1.296_PrNi2B2C | oS | 1.845_Sr2Fe03Cl | oS |
| 0.650_ErSi207 | S | 1.298_BaCdVO(P04)2 | M | 1.846_LaCu3Fe4012 | Lt |
| 0.651_Er3Cu4Sn4 | oS | 1.301_BiMnTe06 | M | 1.849_Na3Ni2Sb06 | Lp |
| 0.658_BaCuTe206 | M | 1.302_Ba2Co04 | M | 1.853_Ba2YFe05 | M |
| 0.665_CeMnSb0 | oS* | 1.304_ZnMn03 | Lp | 1.854_CoTeMo06 | M |
| 0.667_LaMnSb0 | oS* | 1.305_Mn5Si3 | oS | 1.855_Mn3GaC | Lp |
| 0.681_Ce4Sb3 | Lp | 1.306_Na2BaMn(V04)2 | M | 1.856_Mn3GaC | Lp |
| 0.692_Ba4Ru3010 | oS | 1.308_MnBi2Te4 | oS* | 1.857_Li2CoCl4 | oS |
| 0.693_Ba4Ru3010 | oS | 1.311_BaMo(P04)2 | Lp | 2.2_Sr2F2Fe20S2 | Lp |
| 0.694_Bi2Cu04 | oS | 1.312_HoNi2B2C | oS | 2.6_Nd2Cu04 | oS* |
| 0.695_Bi2Cu04 | oS | 1.314_NaFeSi206 | S | 2.7_Sm2Cu04 | oS* |
| 0.706_Tb2Ir3Ga9 | oS | 1.318_Sr2Ru0.95Fe0.0504 | Lt | 2.13_UP | Lp |
| 0.708_CrNb4S8 | oS* | 1.319_Sr2Ru0.95Fe0.0504 | Lt | 2.14_NdMg | Lp |
| 0.712_VNb3S6 | oS* | 1.320_Sr2FeW06 | M | 2.20_UAs | Lt |
| 0.714_Li2Ni(SO4)2 | S* | 1.321_Ba2FeW06 | Lp | 2.21_TbOOH | M |
| 0.723_YbCl3 | S | 1.334_Pr2Pd2In | Lp | 2.22_FeTa206 | Lp |
| 0.724_BaCoSi04 | M | 1.338_U2Ni2In | oS | 2.23_Sr2Co02Ag2Se2 | S |
| 0.728_MoP3Si011 | S | 1.339_EuAs3 | oS | 2.24_Ba2Co02Ag2Se2 | S |
| 0.733_AgRu03 | oS* | 1.340_LuMn03 | M | 2.30_CeRh2Si2 | Lt |
| 0.740_Dy3Ga5012 | oS | 1.341_TmMn03 | Lp | 2.31_Mn3ZnN | M |
| 0.741_Er3Ga5012 | oS | 1.345_NaMnF4 | M | 2.35_CrSe | M |
| 0.743_Ho3Al5012 | oS | 1.346_TlMnF4 | oS* | 2.36_TbGe3 | Lt |
| 0.744_Tb3Al5012 | oS | 1.347_CuFe02 | Lt | 2.48_Pr2Cu04 | oS* |
| 0.745_Ho3Ga5012 | oS | 1.349_CoNb3S6 | Lp | 2.49_La202Fe20Se2 | Lp |
| 0.746_Tb3Ga5012 | oS | 1.354_EuNi03 | Lp | 2.56_La202Fe20S2 | Lp |
| 0.755_Mn2Se03F2 | oS | 1.356_Ho3Ge4 | oS | 2.66_FeSn2 | M |
| 0.757_CeFe03 | oS* | 1.361_DyGe | Lp | 2.67_FeSn2 | M |
| 0.758_CeFe03 | oS | 1.363_TbCu2Si2 | Lp | 2.68_FeGe2 | M |
| 0.760_FeOHS04 | oS* | 1.364_HoCu2Si2 | Lp | 2.71_HoRh | M |
| 0.761_SrFe2Se20 | M | 1.365_TbCu2Si2 | Lp | 2.73_BaNd2Zn05 | M |
| 0.762_SrFe2S20 | M | 1.366_HoCu2Si2 | Lp | 2.77_Eu2Cu04 | oS* |
| 0.766_YbMnSb2 | oS* | 1.367_Pu203 | Lp | 2.78_Nd2Cu04 | oS |
| 0.769_YbMnBi2 | oS | 1.368_Tb2Ni3Si5 | oS | 2.86_FeTa206 | Lp |
| 0.782_NdSc03 | M | 1.369_HFe2Ge2 | Lp | 2.87_TbCoGa5 | M |
| 0.783_NdIn03 | M | 1.370_Li2Cu02 | oS* | 2.88_UNiGa | Lt |
| 0.784_NdCo03 | oS | 1.371_Nd2Ni04 | oS* | 2.93_CoCr04 | M |
| 0.786_NdV03 | S* | 1.374_HoNiGe | M | 2.96_GdMn2Si2 | M |
| 0.787_YV03 | oS* | 1.375_CeScGe | S | 2.99_TbNi1Al | Lt |
| 0.795_Sr2YRu06 | S* | 1.377_CeScSi | S | 2.101_TbSbTe | Lt |
| 0.798_MnPd2 | oS* | 1.379_ErNiGe | Lp | 2.102_TbSbTe | Lt |
| 0.800_MnTe | oS* | 1.380_Sr2Fe03Cl | oS* | 2.104_BaNd2ZnS5 | M |

TABLE IV (*cont.*)

| No. | Class | No. | Class | No. | Class |
|-----------------|-------|---------------------|-------|------------------|-------|
| 0.801_Tl3Fe2S4 | oS | 1.381_Sr2Fe03Br | oS* | 2.106_CaCo3V4012 | Lt |
| 0.802_CuFeS2 | oS* | 1.382_Ca2Fe03Cl | oS* | 2.107_DyTe3 | Lt |
| 0.803_NbMnP | M | 1.383_Ca2Fe03Br | oS* | 2.116_Na3Co2Sb06 | Lt |
| 0.804_MoP3Si011 | S | 1.384_USb2 | oS | 3.1_TmAgGe | Lt |
| 0.815_MnNb206 | oS | 1.385_Sr2Fe03F | oS | 3.2_U02 | oS |
| 0.816_MnTa206 | oS | 1.386_Sr2Fe03F | oS* | 3.4_MgCr204 | M |
| 0.818_MnTa206 | M | 1.387_Sr2Fe03F | oS | 3.6_DyCu | oS |
| 0.819_MnNb206 | M | 1.388_La2Ni03F2 | oS | 3.7_NpBi | oS |
| 0.823_Sr2MnGa05 | oS* | 1.389_Sr2Co03Cl | Lp | 3.8_NdZn | oS |
| 0.825_Ca2MnGa05 | oS | 1.397_Cu3Mg(OD)6Br2 | oS | 3.9_NpS | Lt |
| 0.836_DyFe03 | oS* | 1.398_Pr2Cu04 | Lp | 3.10_NpSe | Lt |
| 0.837_DyFe03 | oS | 1.399_Pr2Cu04 | Lp | 3.11_NpTe | Lt |
| 0.838_DyFe03 | oS | 1.400_TbAg2 | Lp | 3.12_USb | oS |
| 0.839_DyFe03 | oS | 1.403_La2Co04 | oS* | 3.13_CeB6 | Lt |
| 0.840_DyFe03 | oS | 1.404_Sr2Cu02Cl2 | Lp | 3.16_Gd2Ti207 | Lt |
| 0.841_DyFe03 | oS | 1.407_Nd2Cu04 | Lp | 3.18_HoRh | oS |
| 0.842_DyAl03 | M | 1.408_Nd2Cu04 | Lp | 3.19_Co0 | Lt |
| 0.854_Gd2Pt207 | Lp | 1.409_NaMn02 | Lp | 3.21_TmGa3 | oS |
| 0.862_Eu2Ir207 | oS* | 1.411_EuMn2P2 | oS | 3.22_Eu3Pb0 | oS |
| 0.881_CuMnAs | oS | 1.413_Ce3Ni2Ge7 | oS | 3.24_CaFe3Ti4012 | Lp |
| 0.896_NiCr04 | oS* | 1.414_CeNiGe3 | oS | 3.28_Ni0 | Lt |

[1] I. Žutić, J. Fabian, and S. Das Sarma, Spintronics: Fundamentals and applications, *Rev. Mod. Phys.* **76**, 323 (2004).

[2] A. Hirohata, K. Yamada, Y. Nakatani, I.-L. Prejbeanu, B. Diény, P. Pirro, and B. Hillebrands, Review on spintronics: Principles and device applications, *J. Magn. Magn. Mater.* **509**, 166711 (2020).

[3] E. V. Gomonay and V. M. Loktev, Spintronics of antiferromagnetic systems (review article), *Low Temp. Phys.* **40**, 17 (2014).

[4] T. Jungwirth, X. Marti, P. Wadley, and J. Wunderlich, Antiferromagnetic spintronics, *Nat. Nanotechnol.* **11**, 231 (2016).

[5] V. Baltz, A. Manchon, M. Tsoi, T. Moriyama, T. Ono, and Y. Tserkovnyak, Antiferromagnetic spintronics, *Rev. Mod. Phys.* **90**, 015005 (2018).

[6] S. Fukami, V. O. Lorenz, and O. Gomonay, Antiferromagnetic spintronics, *J. Appl. Phys.* **128**, 070401 (2020).

[7] D. Xiong, Y. Jiang, K. Shi, A. Du, Y. Yao, Z. Guo, D. Zhu, K. Cao, S. Peng, W. Cai, D. Zhu, and W. Zhao, Antiferromagnetic spintronics: An overview and outlook, *Fundam. Res.* **2**, 522 (2022).

[8] X. Chen, T. Higo, K. Tanaka, T. Nomoto, H. Tsai, H. Idzuchi, M. Shiga, S. Sakamoto, R. Ando, H. Kosaki, T. Matsuo, D. Nishio-Hamane, R. Arita, S. Miwa, and S. Nakatsuji, Octupole-driven magnetoresistance in an antiferromagnetic tunnel junction, *Nature* **613**, 490 (2023).

[9] P. Qin, H. Yan, X. Wang, H. Chen, Z. Meng, J. Dong, M. Zhu, J. Cai, Z. Feng, X. Zhou, L. Liu, T. Zhang, Z. Zeng, J. Zhang, C. Jiang, and Z. Liu, Room-temperature magnetoresistance in an all-antiferromagnetic tunnel junction, *Nature* **613**, 485 (2023).

[10] Y. Chen, K. Samanta, N. A. Shahed, H. Zhang, C. Fang, A. Ernst, E. Y. Tsymbal, and S. S. P. Parkin, Twist-assisted all-antiferromagnetic tunnel junction in the atomic limit, *Nature* **632**, 1045 (2024).

[11] J. Shi, S. Arpacı, V. Lopez-Dominguez, V. K. Sangwan, F. Mahfouzi, J. Kim, J. G. Athas, M. Hamdi, C. Aygen, H. Arava, C. Phatak, M. Carpentieri, J. S. Jiang, M. A. Grayson, N. Kioussis, G. Finocchio, M. C. Hersam, and P. Khalili Amiri, Electrically controlled all-antiferromagnetic tunnel junctions on silicon with large room-temperature magnetoresistance, *Adv. Mater.* **36**, 2312008 (2024).

[12] P. Wadley, B. Howells, J. Železný, C. Andrews, V. Hills, R. P. Campion, V. Novák, K. Olejník, F. Maccherozzi, S. S. Dhesi, S. Y. Martin, T. Wagner, J. Wunderlich, F. Freimuth, Y. Mokrousov, J. Kuneš, J. S. Chauhan, M. J. Grzybowski, A. W. Rushforth, K. W. Edmonds, B. L. Gallagher, and T. Jungwirth, *Science* **351**, 587 (2016).

[13] M. J. Grzybowski, P. Wadley, K. W. Edmonds, R. Beardsley, V. Hills, R. P. Campion, B. L. Gallagher, J. S. Chauhan, V. Novak, T. Jungwirth, F. Maccherozzi, and S. S. Dhesi, Imaging current-induced switching of antiferromagnetic domains in cunmas, *Phys. Rev. Lett.* **118**, 057701 (2017).

[14] S. Y. Bodnar, L. Šmejkal, I. Turek, T. Jungwirth, O. Gomonay, J. Sinova, A. A. Sapozhnik, H.-J. Elmers, M. Kläui, and M. Jourdan, Writing and reading antiferromagnetic Mn₂Au by Néel spin-orbit torques and large anisotropic magnetoresistance, *Nat. Commun.* **9**, 348 (2018).

[15] X. Z. Chen, R. Zarzuela, J. Zhang, C. Song, X. F. Zhou, G. Y. Shi, F. Li, H. A. Zhou, W. J. Jiang, F. Pan, and Y. Tserkovnyak, Antidamping-torque-induced switching in biaxial antiferromagnetic insulators, *Phys. Rev. Lett.* **120**, 207204 (2018).

[16] M. Meinert, D. Graulich, and T. Matalla-Wagner, Electrical switching of antiferromagnetic Mn₂Au and the role of thermal activation, *Phys. Rev. Appl.* **9**, 064040 (2018).

[17] L. Baldrati, O. Gomonay, A. Ross, M. Filianina, R. Lebrun, R. Ramos, C. Leveille, F. Fuhrmann, T. R. Forrest, F. Maccherozzi, S. Valencia, F. Kronast, E. Saitoh, J. Sinova, and M. Kläui, Mechanism of Néel order switching in antiferromagnetic thin films revealed by magnetotransport and direct imaging, *Phys. Rev. Lett.* **123**, 177201 (2019).

[18] H. Tsai, T. Higo, K. Kondou, T. Nomoto, A. Sakai, A. Kobayashi, T. Nakano, K. Yakushiji, R. Arita, S. Miwa, Y. Otani, and S. Nakatsuji, Electrical manipulation of a topological antiferromagnetic state, *Nature* **580**, 608 (2020).

[19] S. DuttaGupta, A. Kurenkov, O. A. Tretiakov, G. Krishnaswamy, G. Sala, V. Krizakova, F. Maccherozzi, S. S. Dhesi, P. Gambardella, S. Fukami, and H. Ohno, Spin-orbit torque switching of an antiferromagnetic metallic heterostructure, *Nat. Commun.* **11**, 5715 (2020).

[20] S. Arpacı, V. Lopez-Dominguez, J. Shi, L. Sánchez-Tejerina, F. Garesci, C. Wang, X. Yan, V. K. Sangwan, M. A. Grayson, M. C. Hersam, G. Finocchio, and P. Khalili Amiri, Observation of current-induced switching in non-collinear antiferromagnetic IrMn₃ by differential voltage measurements, *Nat. Commun.* **12**, 3828 (2021).

[21] T. Hajiri, K. Matsuura, K. Sonoda, E. Tanaka, K. Ueda, and H. Asano, Spin-orbit-torque switching of non-collinear antiferromagnetic antiperovskite manganese nitride Mn₃GaN, *Phys. Rev. Appl.* **16**, 024003 (2021).

[22] T. Higo, K. Kondou, T. Nomoto, M. Shiga, S. Sakamoto, X. Chen, D. Nishio-Hamane, R. Arita, Y. Otani, S. Miwa, and S. Nakatsuji, Perpendicular full switching of chiral antiferromagnetic order by current, *Nature* **607**, 474 (2022).

[23] M. J. Grzybowski, C. F. Schippers, M. E. Bal, K. Rubi, U. Zeitler, M. Foltyn, B. Koopmans, and H. J. M. Swagten, Electrical switching of antiferromagnetic CoO | Pt across the Néel temperature, *Appl. Phys. Lett.* **120**, 122405 (2022).

[24] G. K. Krishnaswamy, G. Sala, B. Jacot, C.-H. Lambert, R. Schlitz, M. D. Rossell, P. Nöel, and P. Gambardella, Time-dependent multistate switching of topological antiferromagnetic order in Mn₃Sn, *Phys. Rev. Appl.* **18**, 024064 (2022).

[25] Y. Deng, X. Liu, Y. Chen, Z. Du, N. Jiang, C. Shen, E. Zhang, H. Zheng, H.-Z. Lu, and K. Wang, All-electrical switching of a topological non-collinear antiferromagnet at room temperature, *Natl. Sci. Rev.* **10**, nwac154 (2022).

[26] T. Xu, H. Bai, Y. Dong, L. Zhao, H.-A. Zhou, J. Zhang, X.-X. Zhang, and W. Jiang, Robust spin torque switching of noncollinear antiferromagnet Mn₃Sn, *APL Mater.* **11**, 071116 (2023).

[27] H. Song, D. Wang, Y. Xing, W. Zhao, C. Qi, L. Wei, S. Yan, Y. Tian, L. Bai, and Y. Chen, High switch-
ing ratio of antiferromagnetic order in thick sputtered Mn_{3+x}Sn_{1-x} films by spin-orbit torque, *Appl. Phys. Lett.* **125**, 122406 (2024).

[28] Y. Zhang, H. Bai, J. Dai, L. Han, C. Chen, S. Liang, Y. Cao, Y. Zhang, Q. Wang, W. Zhu, F. Pan, and C. Song, Electrical manipulation of spin splitting torque in altermagnetic RuO₂, *Nat. Commun.* **16**, 5646 (2025).

[29] J.-Y. Yoon, Y. Takeuchi, R. Takechi, J. Han, T. Uchimura, Y. Yamane, S. Kanai, J. Ieda, H. Ohno, and S. Fukami, Electrical mutual switching in a noncollinear-antiferromagnetic-ferromagnetic heterostructure, *Nature Communications* **16**, 1171 (2025).

[30] S. Nakatsuji, N. Kiyohara, and T. Higo, Large anomalous hall effect in a non-collinear antiferromagnet at room temperature, *Nature* **527**, 212 (2015).

[31] K. Kuroda, T. Tomita, M.-T. Suzuki, C. Bareille, A. A. Nugroho, P. Goswami, M. Ochi, M. Ikhlas, M. Nakayama, S. Akebi, R. Noguchi, R. Ishii, N. Inami, K. Ono, H. Kumigashira, A. Varykhalov, T. Muro, T. Koretsune, R. Arita, S. Shin, T. Kondo, and S. Nakatsuji, Evidence for magnetic weyl fermions in a correlated metal, *Nat. Mater.* **16**, 1090 (2017).

[32] A. K. Nayak, J. E. Fischer, Y. Sun, B. Yan, J. Karel, A. C. Komarek, C. Shekhar, N. Kumar, W. Schnelle, J. Kübler, C. Felser, and S. S. P. Parkin, Large anomalous hall effect driven by a nonvanishing berry curvature in the noncollinear antiferromagnet Mn₃Ge, *Sci. Adv.* **2**, e1501870 (2016).

[33] N. Kiyohara, T. Tomita, and S. Nakatsuji, Giant anomalous hall effect in the chiral antiferromagnet Mn₃Ge, *Phys. Rev. Appl.* **5**, 064009 (2016).

[34] H. Iwaki, M. Kimata, T. Ikebuchi, Y. Kobayashi, K. Oda, Y. Shiota, T. Ono, and T. Moriyama, Large anomalous hall effect in L1₂-ordered antiferromagnetic Mn₃Ir thin films, *Appl. Phys. Lett.* **116**, 022408 (2020).

[35] N. An, M. Tang, S. Hu, H. Yang, W. Fan, S. Zhou, and X. Qiu, Structure and strain tunings of topological anomalous hall effect in cubic noncollinear antiferromagnet Mn₃Pt epitaxial films, *Sci. China Phys. Mech. Astron.* **63**, 297511 (2020).

[36] L. Šmejkal, J. Sinova, and T. Jungwirth, Emerging research landscape of altermagnetism, *Phys. Rev. X* **12**, 040501 (2022).

[37] L. Šmejkal, J. Sinova, and T. Jungwirth, Beyond conventional ferromagnetism and antiferromagnetism: A phase with nonrelativistic spin and crystal rotation symmetry, *Phys. Rev. X* **12**, 031042 (2022).

[38] L. Bai, W. Feng, S. Liu, L. Šmejkal, Y. Mokrousov, and Y. Yao, Altermagnetism: Exploring new frontiers in magnetism and spintronics, *Adv. Funct. Mater.* **34**, 2409327 (2024).

[39] C. Song, H. Bai, Z. Zhou, L. Han, H. Reichlova, J. H. Dil, J. Liu, X. Chen, and F. Pan, Altermagnets as a new class of functional materials, *Nat. Rev. Mater.* **10**, 473 (2025).

[40] R. Tamang, S. Gurung, D. P. Rai, S. Brahim, and S. Lounis, Altermagnetism and altermagnets: A brief review, *Magnetism* **5**, 10.3390/magnetism5030017 (2025).

[41] D. Rathore, Altermagnetism: Symmetry-driven spin splitting and its role in spintronic technologies, *J. Alloys Compd.* **1034**, 181292 (2025).

[42] T. Jungwirth, J. Sinova, P. Wadley, D. Kriegner, H. Reichlova, F. Krizek, H. Ohno, and L. Šmejkal, *Altermagnetism: Symmetry-driven spin splitting and its role in spintronic technologies*, *J. Alloys Compd.* **1034**, 181292 (2025).

magnetic spintronics (2025), arXiv:2508.09748 [cond-mat.mtrl-sci].

[43] S. Bhowal and A. Bose, Non-relativistic spin splitting: Features and functionalities (2025), arXiv:2510.20306 [cond-mat.mtrl-sci].

[44] S. Hayami, Y. Yanagi, and H. Kusunose, Momentum-dependent spin splitting by collinear antiferromagnetic ordering, *J. Phys. Soc. Jpn.* **88**, 123702 (2019).

[45] M. Naka, S. Hayami, H. Kusunose, Y. Yanagi, Y. Motome, and H. Seo, Spin current generation in organic antiferromagnets, *Nat. Commun.* **10**, 4305 (2019).

[46] L.-D. Yuan, Z. Wang, J.-W. Luo, E. I. Rashba, and A. Zunger, Giant momentum-dependent spin splitting in centrosymmetric low- z antiferromagnets, *Phys. Rev. B* **102**, 014422 (2020).

[47] L.-D. Yuan, Z. Wang, J.-W. Luo, and A. Zunger, Prediction of low- z collinear and noncollinear antiferromagnetic compounds having momentum-dependent spin splitting even without spin-orbit coupling, *Phys. Rev. Mater.* **5**, 014409 (2021).

[48] A. B. Hellenes, T. Jungwirth, R. Jaeschke-Ubiergo, A. Chakraborty, J. Sinova, and L. Šmejkal, *P*-wave magnets (2024), arXiv:2309.01607 [cond-mat.mes-hall].

[49] B. Brekke, P. Sukhachov, H. G. Giil, A. Brataas, and J. Linder, Minimal models and transport properties of unconventional *p*-wave magnets, *Phys. Rev. Lett.* **133**, 236703 (2024).

[50] Q. Song, S. Stavrić, P. Barone, A. Droghetti, D. S. Antonenko, J. W. F. Venderbos, C. A. Occhialini, B. Ilyas, E. Ergeçen, N. Gedik, S.-W. Cheong, R. M. Fernandes, S. Picozzi, and R. Comin, Electrical switching of a *p*-wave altermagnet, *Nature* **642**, 64 (2025).

[51] R. Yamada, M. T. Birch, P. R. Baral, S. Okumura, R. Nakano, S. Gao, M. Ezawa, T. Nomoto, J. Masell, Y. Ishihara, K. K. Kolincio, I. Belopolski, H. Sagayama, H. Nakao, K. Ohishi, T. Ohhara, R. Kiyanagi, T. Nakajima, Y. Tokura, T.-h. Arima, Y. Motome, M. M. Hirschmann, and M. Hirschberger, A metallic *p*-wave magnet with commensurate spin helix, *Nature* **646**, 837 (2025).

[52] J. Matsuda, H. Watanabe, and R. Arita, Multiferroic collinear antiferromagnets with hidden altermagnetic spin splitting, *Phys. Rev. Lett.* **134**, 226703 (2025).

[53] Y. Yu, M. B. Lyngby, T. Shishidou, M. Roig, A. Kreisel, M. Weinert, B. M. Andersen, and D. F. Agterberg, Odd-parity magnetism driven by antiferromagnetic exchange, *Physical Review Letters* **135**, 046701 (2025).

[54] H. Chen, Q. Niu, and A. H. MacDonald, Anomalous hall effect arising from noncollinear antiferromagnetism, *Phys. Rev. Lett.* **112**, 017205 (2014).

[55] J. Kübler and C. Felser, Non-collinear antiferromagnets and the anomalous hall effect, *Europhys. Lett.* **108**, 67001 (2014).

[56] J. Balluff, K. Diekmann, G. Reiss, and M. Meinhert, High-throughput screening for antiferromagnetic heusler compounds using density functional theory, *Phys. Rev. Mater.* **1**, 034404 (2017).

[57] M. K. Horton, J. H. Montoya, M. Liu, and K. A. Persson, High-throughput prediction of the ground-state collinear magnetic order of inorganic materials using density functional theory, *npj Comput. Mater.* **5**, 64 (2019).

[58] A. Sakai, S. Minami, T. Koretsune, T. Chen, T. Higo, Y. Wang, T. Nomoto, M. Hirayama, S. Miwa, D. Nishio, Hamane, F. Ishii, R. Arita, and S. Nakatsuji, Iron-based binary ferromagnets for transverse thermoelectric conversion, *Nature* **581**, 53 (2020).

[59] X. Zhang, W. Meng, Y. Liu, X. Dai, G. Liu, and L. Kou, Magnetic electrides: High-throughput material screening, intriguing properties, and applications, *J. Am. Chem. Soc.* **145**, 5523 (2023), pMID: 36823736.

[60] H. Wang, Q. Feng, S. Li, W. Lin, W. Zhu, Z. Chen, Z. Li, X. Liu, and X. Li, High-throughput screening of ferrimagnetic semiconductors with ultrahigh Néel temperature, *Phys. Rev. Mater.* **9**, 054403 (2025).

[61] H. Liu, J.-T. Sun, M. Liu, and S. Meng, Screening magnetic two-dimensional atomic crystals with nontrivial electronic topology, *J. Phys. Chem. Lett.* **9**, 6709 (2018).

[62] F. Zheng and P. Zhang, Maggene: A genetic evolution program for magnetic structure prediction, *Comput. Phys. Commun.* **259**, 107659 (2021).

[63] E. F. Bertaut, Representation analysis of magnetic structures, *Acta Crystallogr. A* **24**, 217 (1968).

[64] E. Bertaut, On group theoretical techniques in magnetic structure analysis, *J. Magn. Magn. Mater.* **24**, 267 (1981).

[65] Y. Izyumov and V. Naish, Symmetry analysis in neutron diffraction studies of magnetic structures: 1. a phase transition concept to describe magnetic structures in crystals, *J. Magn. Magn. Mater.* **12**, 239 (1979).

[66] W. Opechowski and T. Dreyfus, Classifications of magnetic structures, *Acta Crystallogr. A* **27**, 470 (1971).

[67] V. Petříček, J. Fuksa, and M. Dušek, Magnetic space and superspace groups, representation analysis: competing or friendly concepts?, *Acta Crystallogr. A* **66**, 649 (2010).

[68] J. Rodriguez-Carvajal and J. M. Perez-Mato, Magnetic space groups *versus* representation analysis in the investigation of magnetic structures: the happy end of a strained relationship, *Acta Crystallogr. B* **80**, 370 (2024).

[69] M.-T. Huebsch, T. Nomoto, M.-T. Suzuki, and R. Arita, Benchmark for ab initio prediction of magnetic structures based on cluster-multipole theory, *Phys. Rev. X* **11**, 011031 (2021).

[70] B. J. Campbell, H. T. Stokes, D. E. Tanner, and D. M. Hatch, *ISODISPLACE*: a web-based tool for exploring structural distortions, *J. Appl. Crystallogr.* **39**, 607 (2006).

[71] J. Perez-Mato, S. Gallego, E. Tasci, L. Elcoro, G. de la Flor, and M. Aroyo, Symmetry-based computational tools for magnetic crystallography, *Annu. Rev. Mater. Res.* **45**, 217 (2015).

[72] H. T. Stokes and D. M. Hatch, *Isotropy Subgroups of the 230 Crystallographic Space Groups* (WORLD SCIENTIFIC, Singapore, 1989).

[73] E. Ascher, Permutation representations, epikernels and phase transitions, *J. Phys. C: Solid State Phys.* **10**, 1365 (1977).

[74] M.-T. Suzuki, T. Koretsune, M. Ochi, and R. Arita, Cluster multipole theory for anomalous hall effect in antiferromagnets, *Phys. Rev. B* **95**, 094406 (2017).

[75] M.-T. Suzuki, T. Nomoto, R. Arita, Y. Yanagi, S. Hayami, and H. Kusunose, Multipole expansion for magnetic structures: A generation scheme for a symmetry-adapted orthonormal basis set in the crystallographic point group, *Phys. Rev. B* **99**, 174407 (2019).

[76] Y. Yanagi, H. Kusunose, T. Nomoto, R. Arita, and M.-T. Suzuki, Generation of modulated magnetic structures based on cluster multipole expansion: Application to α -Mn and CoM_3S_6 , *Phys. Rev. B* **107**, 014407 (2023).

[77] T. Nomoto, S. Minami, Y. Yanagi, M.-T. Suzuki, T. Koresune, and R. Arita, High-throughput calculations of antiferromagnets hosting anomalous transport phenomena, *Phys. Rev. B* **109**, 094435 (2024).

[78] P. Liu, J. Li, J. Han, X. Wan, and Q. Liu, Spin-group symmetry in magnetic materials with negligible spin-orbit coupling, *Phys. Rev. X* **12**, 021016 (2022).

[79] H. Watanabe, K. Shinohara, T. Nomoto, A. Togo, and R. Arita, Symmetry analysis with spin crystallographic groups: Disentangling effects free of spin-orbit coupling in emergent electromagnetism, *Phys. Rev. B* **109**, 094438 (2024).

[80] Y. Jiang, Z. Song, T. Zhu, Z. Fang, H. Weng, Z.-X. Liu, J. Yang, and C. Fang, Enumeration of spin-space groups: Toward a complete description of symmetries of magnetic orders, *Phys. Rev. X* **14**, 031039 (2024).

[81] Z. Xiao, J. Zhao, Y. Li, R. Shindou, and Z.-D. Song, Spin space groups: Full classification and applications, *Phys. Rev. X* **14**, 031037 (2024).

[82] X. Chen, J. Ren, Y. Zhu, Y. Yu, A. Zhang, P. Liu, J. Li, Y. Liu, C. Li, and Q. Liu, Enumeration and representation theory of spin space groups, *Phys. Rev. X* **14**, 031038 (2024).

[83] W. Brinkman and R. J. Elliott, Space group theory for spin waves, *J. Appl. Phys.* **37**, 1457 (1966).

[84] W. F. Brinkman and R. J. Elliott, Theory of spin-space groups, *Proc. Math. Phys. Eng. Sci.* **294**, 343 (1966).

[85] D. B. Litvin, Spin translation groups and neutron diffraction analysis, *Acta Crystallogr. A* **29**, 651 (1973).

[86] D. Litvin and W. Opechowski, Spin groups, *Physica* **76**, 538 (1974).

[87] D. B. Litvin, Spin point groups, *Acta Crystallogr. A* **33**, 279 (1977).

[88] W. Opechowski, *Crystallographic and Metacrystallographic Groups* (North-Holland, 1986).

[89] Y. A. Izyumov, V. E. Naish, and R. P. Ozerov, *Neutron Diffraction of Magnetic Materials* (Springer New York, New York, NY, 1991).

[90] J. Železný, Y. Zhang, C. Felser, and B. Yan, Spin-polarized current in noncollinear antiferromagnets, *Phys. Rev. Lett.* **119**, 187204 (2017).

[91] Y. Zhang, J. Železný, Y. Sun, J. van den Brink, and B. Yan, Spin Hall effect emerging from a noncollinear magnetic lattice without spin-orbit coupling, *New journal of physics* **20**, 073028 (2018).

[92] H. Schiff, A. Corticelli, A. Guerreiro, J. Romhányi, and P. McClarty, The crystallographic spin point groups and their representations, *SciPost Phys.* **18**, 109 (2025).

[93] S. Zhang, Z. Song, Z. Fang, H. Weng, and Z. Wang, Irrsg: An open-source software package for spin space groups (2025), arXiv:2511.21821 [cond-mat.mtrl-sci].

[94] Z. Song, A. Z. Yang, Y. Jiang, Z. Fang, J. Yang, C. Fang, H. Weng, and Z.-X. Liu, Constructions and applications of irreducible representations of spin-space groups, *Phys. Rev. B* **111**, 134407 (2025).

[95] P. A. McClarty and J. G. Rau, Landau theory of altermagnetism, *Phys. Rev. Lett.* **132**, 176702 (2024).

[96] J. Etxebarria, J. M. Perez-Mato, E. S. Tasci, and L. Elcoro, Crystal tensor properties of magnetic materials with and without spin-orbit coupling. Application of spin point groups as approximate symmetries, *Acta Crystallogr. A* **81**, 317 (2025).

[97] R.-C. Xiao, Y. Jin, Z.-F. Zhang, Z.-H. Feng, D.-F. Shao, and M. Tian, Tensorsymmetry: a package to get symmetry-adapted tensors disentangling spin-orbit coupling effect and establishing analytical relationship with magnetic order, *Comput. Phys. Commun.* **318**, 109872 (2026).

[98] L. Elcoro, J. Etxebarria, J. M. Perez-Mato, and E. S. Tasci, Automatic calculation of symmetry-adapted tensors under spin-group symmetry. stensor, a new tool of the bilbao crystallographic server (2026), arXiv:2601.01140 [cond-mat.mtrl-sci].

[99] Y. Liu, X. Chen, Y. Yu, and Q. Liu, Symmetry classification of magnetic orders and emergence of spin-orbit magnetism (2025), arXiv:2506.20739 [cond-mat.mtrl-sci].

[100] S. V. Gallego, J. M. Perez-Mato, L. Elcoro, E. S. Tasci, R. M. Hanson, K. Momma, M. I. Aroyo, and G. Madariaga, MAGNDATA: towards a database of magnetic structures. I. The commensurate case, *J. Appl. Crystallogr.* **49**, 1750 (2016).

[101] S. V. Gallego, J. M. Perez-Mato, L. Elcoro, E. S. Tasci, R. M. Hanson, M. I. Aroyo, and G. Madariaga, MAGNDATA: towards a database of magnetic structures. II. The incommensurate case, *J. Appl. Crystallogr.* **49**, 1941 (2016).

[102] Y. Li, S. Zeng, X. Chen, R. Xiong, Y. Yu, Y.-J. Zhao, and Q. Liu, Symmetry-guided prediction of magnetic-ordered ground states (2025), arXiv:2512.21672 [cond-mat.mtrl-sci].

[103] K. Shinohara, A. Togo, H. Watanabe, T. Nomoto, I. Tanaka, and R. Arita, Algorithm for spin symmetry operation search, *Acta Crystallogr. A* **80**, 94 (2024).

[104] É. Goursat, Sur les substitutions orthogonales et les divisions régulières de l'espace, *Ann. Sci. Éc. Norm. Supér.* **3**, 6, 9 (1889).

[105] C. Hermann, XXXV. zur systematischen strukturtheorie., *Z. Kristallogr. Cryst. Mater.* **69**, 533 (1929).

[106] W. Opechowski, Metacrystallographic groups, in *Group Theoretical Methods in Physics*, edited by R. T. Sharp and B. Kolman (Academic Press, 1977) pp. 93–113.

[107] Rodríguez-Carvajal, J. and Bourée, F., Symmetry and magnetic structures, *EPJ Web Conf.* **22**, 00010 (2012).

[108] H. Wondratschek, Splitting of wyckoff positions (orbits), *Mineralogy and Petrology* **48**, 87 (1993).

[109] K. Shinohara, A. Togo, and I. Tanaka, Algorithms for magnetic symmetry operation search and identification of magnetic space group from magnetic crystal structure, *Acta Crystallogr. A* **79**, 390 (2023).

[110] H. D. Flack, Chiral and achiral crystal structures, *Helv. Chim. Acta* **86**, 905 (2003).

[111] V. Moneti, M. Loire, and R. Ballou, Magnetic chirality as probed by neutron scattering, *Eur. Phys. J. Spec. Top.* **213**, 5 (2012).

[112] S.-W. Cheong and X. Xu, Magnetic chirality, *npj Quantum Mater.* **7**, 40 (2022).

[113] S. Pradhan, K. Samanta, K. Saha, and A. K. Nandy, Vector-chirality driven topological phase transitions in noncollinear antiferromagnets and its impact on anomalous hall effect, *Commun. Phys.* **6**, 272 (2023).

[114] J. Villain, Two-level systems in a spin-glass model. i. general formalism and two-dimensional model, *J. Phys.*

C: Solid State Phys. **10**, 4793 (1977).

[115] M. Kaburagi, H. Kawamura, and T. Hikihara, Spin and chiral orderings of frustrated quantum spin chains, *J. Phys. Soc. Jpn.* **68**, 3185 (1999).

[116] L. Arnaut, Chirality in multi-dimensional space with application to electromagnetic characterisation of multi-dimensional chiral and semi-chiral media, *J. Electromagn. Wave Appl.* **11**, 1459 (1997).

[117] L. D. Barron, An introduction to chirality at the nanoscale, in *Chirality at the Nanoscale* (John Wiley & Sons, Ltd, 2009) Chap. 1, pp. 1–27.

[118] Kunitomi, Nobuhiko, Hamaguchi, Yoshikazu, and Anzai, Shuichiro, Neutron diffraction study on manganese telluride, *J. Phys. France* **25**, 568 (1964).

[119] N. V. Belov, N. N. Neronova, and T. S. Smirnova, Shubnikov groups, Sov. Phys. Crystallogr. **2**, 311 (1957).

[120] P. J. Brown, V. Nunez, F. Tasset, J. B. Forsyth, and P. Radhakrishna, Determination of the magnetic structure of mn3sn using generalized neutron polarization analysis, *J. Phys. Condens. Matter* **2**, 9409 (1990).

[121] H. Takagi, R. Takagi, S. Minami, T. Nomoto, K. Ohishi, M.-T. Suzuki, Y. Yanagi, M. Hirayama, N. D. Khanh, K. Karube, H. Saito, D. Hashizume, R. Kiyanagi, Y. Tokura, R. Arita, T. Nakajima, and S. Seki, Spontaneous topological hall effect induced by non-coplanar antiferromagnetic order in intercalated van der waals materials, *Nat. Phys.* **19**, 961 (2023).

[122] K. Shinohara, moyo: A fast and robust crystal symmetry finder, written in Rust (2026), source code available at <https://github.com/spglib/moyo>.

[123] K. Mathew, J. Montoya, A. Faghaninia, S. Dwarakanath, M. Aykol, H. Tang, I. Chu, T. Smidt, B. Bocklund, M. Horton, J. Dagdelen, B. Wood, Z. Liu, J. Neaton, S. Ong, K. Persson, and A. Jain, Atomate: A high-level interface to generate, execute, and analyze computational materials science workflows, *Comput. Mater. Sci.* **139**, 140 (2017).

[124] A. M. Ganose, H. Sahasrabuddhe, M. Asta, K. Beck, T. Biswas, A. Bonkowski, J. Bustamante, X. Chen, Y. Chiang, D. C. Chrzan, J. Clary, O. A. Cohen, C. Eratural, M. C. Gallant, J. George, S. Gerits, R. E. A. Goodall, R. D. Guha, G. Hautier, M. Horton, T. J. Inizan, A. D. Kaplan, R. S. Kingsbury, M. C. Kuner, B. Li, X. Linn, M. J. McDermott, R. S. Mohanakrishnan, A. N. Naik, J. B. Neaton, S. M. Parmar, K. A. Persson, G. Petretto, T. A. R. Purcell, F. Ricci, B. Rich, J. Riebesell, G.-M. Rignanese, A. S. Rosen, M. Scheffler, J. Schmidt, J.-X. Shen, A. Sobolev, R. Sundararaman, C. Tezak, V. Trinquet, J. B. Varley, D. Vigil-Fowler, D. Wang, D. Waroquiers, M. Wen, H. Yang, H. Zheng, J. Zheng, Z. Zhu, and A. Jain, Atomate2: modular workflows for materials science, *Digit. Discov.* **4**, 1944 (2025).

[125] S. P. Ong, W. D. Richards, A. Jain, G. Hautier, M. Kocher, S. Cholia, D. Gunter, V. L. Chevrier, K. A. Persson, and G. Ceder, Python materials genomics (pymatgen): A robust, open-source python library for materials analysis, *Comput. Mater. Sci.* **68**, 314 (2013).

[126] A. Jain, S. P. Ong, W. Chen, B. Medasani, X. Qu, M. Kocher, M. Brafman, G. Petretto, G.-M. Rignanese, G. Hautier, D. Gunter, and K. A. Persson, Fireworks: a dynamic workflow system designed for high-throughput applications, *Concurr. Comput. Pract. Exp.* **27**, 5037 (2015).

[127] G. Kresse and J. Furthmüller, Efficient iterative schemes for ab initio total-energy calculations using a plane-wave basis set, *Phys. Rev. B* **54**, 11169 (1996).

[128] J. P. Perdew, K. Burke, and M. Ernzerhof, Generalized gradient approximation made simple, *Phys. Rev. Lett.* **77**, 3865 (1996).

[129] P. E. Blöchl, Projector augmented-wave method, *Phys. Rev. B* **50**, 17953 (1994).

[130] G. Kresse and D. Joubert, From ultrasoft pseudopotentials to the projector augmented-wave method, *Phys. Rev. B* **59**, 1758 (1999).

[131] H. Zhou, Y. Mu, D. Zhang, H. Chu, D. Wang, H. Liu, and X. Wan, Magnetic structures database from symmetry-aided high-throughput calculations (2026), arXiv:2601.01617.

[132] K. Momma and F. Izumi, VESTA3 for three-dimensional visualization of crystal, volumetric and morphology data, *J. Appl. Crystallogr.* **44**, 1272 (2011).

[133] L. Pyber, Enumerating finite groups of given order, *Ann. Math.* **137**, 203 (1993).

[134] G. L. W. Hart and R. W. Forcade, *Phys. Rev. B* **77**, 224115 (2008).

[135] H. T. Stokes and B. J. Campbell, A general algorithm for generating isotropy subgroups in superspace, *Acta Crystallogr. A* **73**, 4 (2017).

[136] H. T. Stokes, D. M. Hatch, and J. D. Wells, Group-theoretical methods for obtaining distortions in crystals: Applications to vibrational modes and phase transitions, *Phys. Rev. B* **43**, 11010 (1991).

[137] K. Shinohara, A. Togo, and I. Tanaka, spgrep: On-the-fly generator of space-group irreducible representations, *J. Open Source Softw.* **8**, 5269 (2023).